Available online at www.sciencedirect.com
SCIENCE DIRECT
International Journal of Mass Spectrometry 254 (2006) 1–19
International Journal of Mass Spectrometry
www.elsevier.com/locate/ijms

Review

# Gas-phase infrared multiple photon dissociation spectroscopy of mass-selected molecular ions

Jos Oomens [a], Boris G. Sartakov [a,b], Gerard Meijer [c], Gert von Helden [c,*]

[a] *FOM Institute for Plasma Physics "Rijnhuizen", Edisonbaan 14, 3439MN Nieuwegein, The Netherlands*
[b] *General Physics Institute of the Russian Academy of Sciences, 38 Vavilov Street, 119991 Moscow, Russia*
[c] *Fritz-Haber-Institut der Max-Planck-Gesellschaft, Faradayweg 4-6, D-14195 Berlin, Germany*

Received 14 March 2006; received in revised form 9 May 2006; accepted 9 May 2006

**Abstract**

In this review, we present an overview of our recent work on the infrared spectroscopy of mass-selected gas-phase molecular ions. The ions are stored and isolated in a quadrupole ion trap where they are investigated with infrared multiple photon dissociation spectroscopy using a free electron laser (FEL). The wide and continuous tunability of FELIX, the FEL for Infrared eXperiments at the FOM institute for Plasma Physics in The Netherlands, allows us to explore the interesting mid-infrared range between 500 and 2000 $cm^{-1}$, sometimes referred to as the fingerprint region. The experiments have focused on polycyclic aromatic hydrocarbons because of their hypothesized occurrence in the interstellar medium, both in neutral and cationic forms. Furthermore, several related species of fundamental chemical interest have been investigated, such as molecular fragment ions and protonated species. The spectra are compared to theoretical spectra calculated at the density functional theory level. The effects of multiple photon excitation and dissociation dynamics on the appearance of the spectrum are extensively discussed. A mathematical model to account for the effects of anharmonicity is described. It explains for instance, qualitatively, how the observed spectral response can vary (slightly) with the fragment channel, which allows one to "direct" dissociation reactions in a non-coherent fashion by the choice of the infrared excitation wavelength.


*Keywords:* Infrared; Spectroscopy; Gas-phase ions; Multiple photon dissociation

## Contents



* Corresponding author. Tel.: +49 30 8413 5615; fax: +49 30 8413 5603.
*E-mail address:* helden@fhi-berlin.mpg.de (G. von Helden).

1387-3806/$ – see front matter © 2006 Elsevier B.V. All rights reserved.
doi:10.1016/j.ijms.2006.05.009

## 1. Introduction

Both optical spectroscopy and mass spectrometry have contributed enormously to our present knowledge of the structure and dynamics of atoms and molecules. Infrared spectroscopy has long been, and still is, one of the basic methods for molecular structure characterization and especially with the advent of Fourier Transform spectrometers, sub-wavenumber resolution experiments have become possible with standard, commercially available instruments. Gas-phase measurements can be performed with such instruments by simply placing an absorption cell in the light beam and, very efficiently, spectra covering the entire infrared range can be obtained. Indeed, large databases with infrared spectra of numerous stable molecules are nowadays available. When a higher sensitivity and/or a better spectral resolution is required, laser based methods can be applied; laser based systems can achieve a resolution better than 1 kHz, albeit over a limited spectral range. The sensitivity can be improved substantially by employing frequency modulation and/or cavity enhanced methods (see e.g., [1]). A general problem of direct absorption measurements is their inherently limited sensitivity. For that reason, IR direct absorption spectroscopy is mostly confined to stable species having a sufficient vapor pressure and the number densities required for routine measurements are on the order of $10^{10}$ molecules/cm$^3$ or higher.

Mass spectrometry, its contributions and successes, as well as the methods being used need no introduction in this journal. In the early days, experiments were largely performed by using electron impact ionization of stable neutral molecules that have a sufficient vapor pressure. As those neutral species are mostly electronically closed shell, the corresponding ionic species are open shell and usually very reactive. Ionization methods such as chemical ionization, matrix assisted laser desorption ionization (MALDI) or electrospray ionization (ESI) frequently produce electronically closed shell species where the charge stems from the addition or removal of closed shell cations ($H^+$, $Li^+$, ...) or anions ($F^-$, $Cl^-$, ...). Hence, mass spectrometry and IR spectroscopy traditionally focussed on very different species and, until recently largely evolved on different paths.

Coulombic repulsion in a cloud of ions having the same charge usually limits the obtainable number densities to about $10^6$ ions/cm$^3$. This is many orders of magnitude lower than densities typically used in infrared direct absorption spectroscopy measurements. In some cases, in the early days of infrared ion spectroscopy, this problem could be circumvented by using long pathlength absorption cells, such as White type cells, and/or "massive" ionization methods, being mainly electron impact ionization as well as discharge sources. Interesting examples of those early studies are found in the work by Harold Schwarz [2], Takeshi Oka, who recorded the first infrared spectrum of $H_3^+$ [3], and the work done in the group of Dymanus [4,5] and in the group of Richard Saykally [6,7].

The use of electron impact and discharge ionization methods however has the drawback that it can induce substantial, or even complete, fragmentation of molecules. When a direct absorption spectrum is subsequently recorded, the nature of the absorbing species can be unclear. The introduction of a mass selection device prior to the absorption measurement usually reduces the ion density to an extent that the direct measurement of the absorption is even more difficult and in essentially all cases impossible. Different techniques are thus required to measure the optical properties of dilute charged species in a mass/charge selective manner (see e.g., [8] for a recent review). Those requirements can be satisfied by the use of one of several "action spectroscopy" techniques, where not the direct absorption of the incident light beam is measured, but the response of the molecule to photon absorption. Such a response can be, for example, the emission of photons, fragments or electrons.

With the increasing availability of commercial laser systems by the end of the 1970s, various such techniques had been developed for optical spectroscopy, most notably resonance enhanced multiphoton ionization (REMPI) and laser induced fluorescence (LIF). Being based on ionization and fluorescence, these methods are obviously less amenable to infrared excitation, but it was realized that fragmentation *could* be induced by infrared radiation. The absorption of infrared radiation can induce dissociation of a molecule or complex, and this can be detected by recording the intensity of the resulting fragments in a mass spectrometer. The integration of infrared spectroscopy with mass spectrometry was born.

The earliest experiments were performed on weakly bound molecular clusters that can be generated in a supersonic jet expansion. In the early 1980s, Y.T. Lee and coworkers recorded infrared spectra of protonated hydrogen and water clusters [9–11]. Being only weakly bound, the complexes can be dissociated with a single infrared photon so that relatively low power

laser sources can be utilized (difference frequency generation of a pulsed dye laser was mostly used in the work of Lee). The cluster ions generated in a molecular beam were stored in an octopole trap and after infrared irradiation the wavelength dependent fragment intensity was detected with a quadrupole mass spectrometer. The technique of tagging the molecular ion of interest with a small molecule or (rare gas) atom, solely for the purpose of detecting the absorption of infrared radiation by its detachment, became known as the "messenger technique".

Infrared induced dissociation of more strongly bound species, such as covalently bound molecules, via the absorption of multiple photons [12], is a method that was known mainly from studies aiming at laser isotope separation [13–18]. Infrared multiple photon dissociation (IRMPD) spectroscopy has also been applied to obtain spectra for molecular ions. In the 1980s, Beauchamp at Caltech studied several negatively charged complexes stored in a Fourier Transform Ion Cyclotron (FTICR) mass spectrometer [19,20], and Eyler at the University of Florida studied several charged organic molecules [21,22]. Other variants, applying different ion trapping devices, were also reported [23]. As IRMPD typically requires the absorption of tens to hundreds of photons, this process can only be induced by the most powerful lasers. Gas discharge lasers, and in particular $CO_2$ lasers, have traditionally been used for these studies. However, the applicability of the technique was severely impaired by the limited and discontinuous wavelength tunability of these lasers.

Nonlinear optical techniques allow for the efficient generation of IR light around 3 μm, enabling experiments that probe the hydrogen stretching modes. Such light sources are for example used in the work on the spectroscopic identification of protonation sites by Dopfer and coworkers [24–27], the studies on anionic cluster ions by Bieske and coworkers [27–29], investigations of the structure of hydrogen bonded ionic systems [30–32] including protonated solvent clusters [33,34] by Mikami and coworkers, the hydrated proton and hydroxide ion spectra of Johnson and coworkers [35,36], the work on transition metal ion solvation by Duncan and coworkers [37,38], the hydrated alkali metal ion complexes studied by Lisy and coworkers [39,40], the spectroscopy of protonated and lithiated amino acids and their hydrated clusters by the groups of Rizzo and Williams [41], and the spectroscopic studies of charged peptides and proteins by Breuker, McLafferty, and coworkers [42].

In the 1990s, it was shown that an infrared free electron laser (FEL) can be used to induce multiple photon dissociation in covalently bound molecules [14,15,43,44], and in 2000 we published the first IRMPD spectra of ionic molecules obtained with the help of an FEL [45]. These spectra, which cover the wavenumber range of 500–1700 $cm^{-1}$, were recorded for (strong, covalently bound) polyaromatic ions stored in a quadrupole ion trap. The introduction of more advanced ion trapping devices, coupled to the Orsay FEL as well as to our FEL, allow the study of a wide variety of (bio-)chemically interesting charged species. Particularly the coupling with linear multipole ion traps and Fourier Transform mass spectrometers, equipped with different external ion sources has proven to be very promising. Systems studied include proton bound dimers [46,47], the Zundel ion $H_5O_2^+$ [48,49], protonated as well as alkali metal cationized amino acids and peptides [50–52], various transition metal coordination complexes [53–55], an entire protein representing the largest molecule for which a gas-phase infrared spectrum was ever recorded [56], as well as several anionic species [57–59]. In this paper we review the work performed at FELIX on the infrared spectroscopy of molecular ions stored in a Paul type quadrupole trap; we first describe the experiment, and then give an overview of our studies of cationic polycyclic aromatic hydrocarbon molecules. Next, an extensive discussion of the IRMPD mechanism and its effects on the spectra is presented. Finally, we report on several other systems studied.

## 2. Methods

### 2.1. Experimental

In the following, we give a brief description of the tools and techniques used to perform the experiments. First, we give an overview of the FEL that is used in the studies presented here. We then describe the ion trap, the ionization techniques, and briefly introduce the computational methods used to explain the experiments.

#### 2.1.1. FELIX: the Free Electron Laser for Infrared eXperiments

Being transparent throughout the electromagnetic spectrum, free electrons, i.e., unbound to an atomic nucleus, form an ideal lasing medium. This property has led to the development of free electron lasers (FELs) operating in wavelength ranges from the (extreme) ultraviolet to the far-infrared. Applications of FEL radiation are not only found in spectroscopy but also in material science and processing, biology, medical treatment, etc. [60,61].

Briefly, in an FEL [62,63], free electrons are accelerated to relativistic speeds and injected into a periodic magnetic structure, called undulator or wiggler, as sketched in Fig. 1. The acceleration devices used in most FELs are radio frequency linear accelerators (rf-linacs). They accelerate electrons in packets (bunches) that are typically a few picoseconds long. The periodically alternating direction of the magnetic field in the undulator causes the electrons to undergo a sinusoidal wiggling motion while traversing the undulator. At each change of direction, an electron emits radiation in a continuous frequency band. To obtain coherence in a periodic structure, the electron bunch and the light wave have to be in-phase at each turning point in the wiggling motion. However, since the light wave obviously travels in a straight line at the speed of light, whereas the electron bunch path deviates slightly from that straight line due to the wiggling motion, the electron bunch always lags behind with respect to the light wave. In order to still meet the requirement of coherence, the undulator parameters are chosen such that the lag amounts to exactly one (or an integer number of) wavelength per undulator period. Different electrons will however not necessarily emit in phase with each other and the resulting radiation is thus weak. In order to achieve phase coherence between different electrons, the electron bunches need to be extremely short. To directly gen-

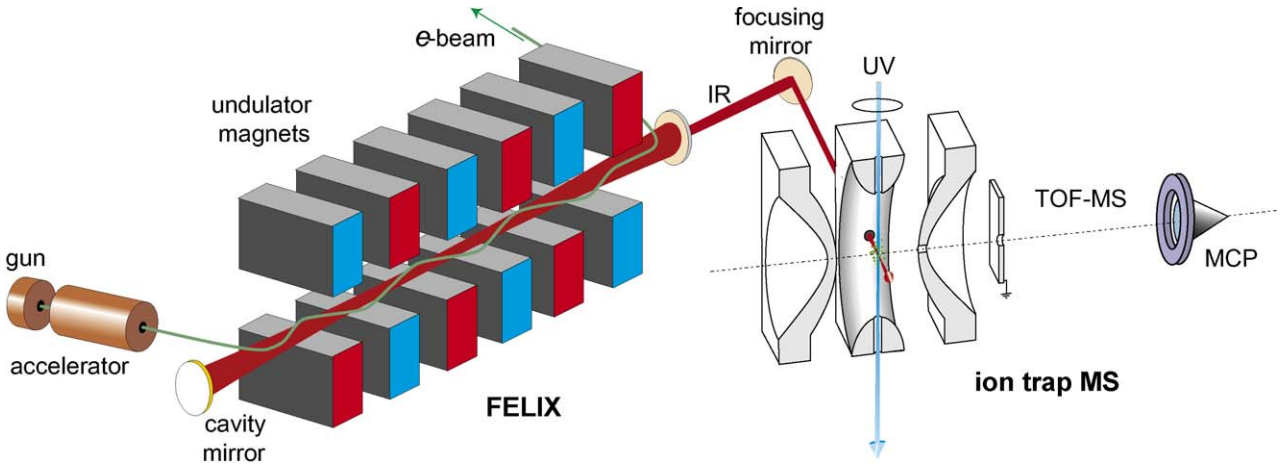


Fig. 1. Artist's impression of the experiment with the free electron laser on the left and the ion trap time-of-flight mass spectrometer on the right. Note that in reality the overall length of the FEL from gun to outcoupling mirror amounts to more than 20 m, whereas the inner diameter of the ion trap measures only 2 cm.

erate such bunches for the desired wavelength is impractical. Bunching can however also occur by interaction of the electrons with the radiation field in the undulator. To this end, the radiation is captured in an optical cavity formed by two spherical mirrors placed around the undulator. A fresh electron bunch that enters the undulator interacts with the radiation field inducing a spatial modulation, i.e., bunching, and the emission of stimulated radiation, which is now coherent, and high gain is achieved. The length of the cavity is sensitively determined by the requirement that freshly injected electron bunches are resonant with the light pulses circulating in the cavity. The amount of deviation that the electrons undergo from the straight path followed by the light wave depends on the magnetic field strength. In other words, the wavelength for which resonance occurs changes as the undulator field strength is altered, and this can be used to tune the lasing wavelength.

The original setup in which the experiments described in this review were carried out consists of a quadrupole ion trap with a time-of-flight (TOF) mass spectrometer interfaced to the beamline of FELIX. A schematic picture is sketched in Fig. 1.

The FEL used in the present studies, FELIX [64], consists of an electron beamline with two separate optical cavities, one for the long (25–250 μm) and one for the short (5–30 μm) wavelength range. The experiments described here are all performed in the short wavelength range, for which the electrons are accelerated to energies up to around 40 MeV, using two linacs. For a given electron energy, the wavelength can be tuned roughly over a factor of 3 by changing the gap between the two arrays of undulator magnets with the use of stepper motors. This construction allows the wavelength to be tuned conveniently and continuously without the intervention of the FEL operator.

FELIX produces radiation in so-called macropulses, typically 5 μs long, which consist of a train of 0.1–10 ps long micropulses. The micropulses are spaced by 1 ns. The macropulse repetition rate used in these experiments is 5 Hz. The bandwidth of the radiation is Fourier Transform limited by the length of the micropulses, and amounts in our experiments to typically 0.5% of the central wavelength. In order to reach wavelengths in the 2.5–5 μm range, FELIX can be operated in the third harmonic mode, which means that electron bunches that lag behind the light wave by exactly three wavelengths are used to generate radiation. This radiation is selectively captured in the cavity by replacing one of the gold-coated mirrors by a dielectrically coated mirror, which is highly reflective at the third harmonic wavelength and transparent at the fundamental. Typical pulse energies are on the order of one-third of those in the fundamental wavelength range.

The IR output of the FEL can be used to induce IRMPD. At appropriate FEL fluences, this IRMPD process only occurs when the IR radiation is resonant with an IR active vibration of the species that is being investigated. Recording the IRMPD efficiency as a function of IR wavelength results thus in an IR spectrum. This spectrum is not necessarily the same as the "normal" linear one photon absorption spectrum, however, it is usually found to be very close to it. This point is further discussed in Section 4.

### 2.1.2. Ion trap mass spectrometer

The ion trap time-of-flight mass spectrometer is similar to the one described by Lubman and coworkers [65]. It consists of a quadrupole "Paul-type" ion trap [66] with a 2-cm inner diameter ring electrode sandwiched between two hyperbolically shaped endcap electrodes (R.M. Jordan Co.). The ring electrode is fed with a 1-MHz rf drive voltage and the entire ion trap is biased at around 850 VDC. To extract ions from the trap, a trigger pulse is given using a delay generator (Stanford Research Systems DG535), which switches off the rf voltage at the next zero-crossing. After a delay of a few rf cycles to minimize residual rf, the bias voltage on one of the endcaps is pulsed down by about 250 V. This endcap has a 3-mm hole in the center, through which the ions are extracted into the linear TOF mass spectrometer. The ion current is recorded on a dual microchannel plate (MCP) detector and is digitized by a 100 MS/s oscilloscope. The data acquisition is synchronized with the dc bias pulse on the endcap.

### 2.1.3. Ionization

Neutral molecules are introduced in the ion trap from an effusive source, an oven containing the solid sample. Since

mostly aromatic systems with an IP of typically 7–8 eV have been studied, ionization is efficiently induced via non-resonant two-photon absorption using an ArF excimer laser ($\lambda = 193$ nm, $E = 6.4$ eV). The laser beam is introduced in the trap via two 2-mm holes drilled into opposite sides of the ring electrode, and is focused in the center of the trap using a lens with a focal length of 20 cm.

The non-resonant ionization process generally causes substantial fragmentation. Along with the ionized parent molecule, the ionic fragmentation products are instantaneously stored in the ion trap. These UV induced fragments would obscure any subsequent IR induced dissociation and therefore, a relatively simple method to eject these fragments before IR irradiation was developed. The rf amplitude can be controlled with a 0–9 VDC input on the Jordan ion trap control. By briefly (≈2 ms) raising the rf amplitude after the UV pulse, the low-mass cut-off of the ion trap can be located just below the parent ion mass, thereby ejecting all lower mass species, i.e., the fragments. After this short increase, the rf amplitude returns to its normal operating voltage so that subsequently, fragments produced by IR irradiation remain trapped and can be analyzed background-free in the TOF mass spectrometer. Note that the dc pulse sequence required to accomplish this can be conveniently produced with the delay generator using the appropriate bias and amplitude settings.

Non-aromatic organic molecules as well as molecules that are unstable under UV irradiation cannot be ionized using this simple method. An efficient alternative in these instances was found in chemical ionization. Two different molecules are vaporized in the chamber, one which can be efficiently ionized with an excimer laser and the other being the molecule of interest. Of course, chemical ionization only occurs if the IP of the molecule of interest is lower than that of the ionized species, which is often not the case. However, in the non-resonant ionization with the focused 193 nm radiation, various small ionic fragments are usually produced, which have a relatively high IP. These ionic fragments drive the chemical ionization to the species of interest. Benzoic acid was found to be a good agent for this indirect ionization method as it yields a fair amount of small ionic fragments. It was used to ionize benzoic acid itself [67], which undergoes complete fragmentation under UV irradiation [68], as well as to ionize adamantane, which does not possess any UV absorption in the excimer laser wavelength range [69]. Depending on the proton affinities of the fragments and the species under study, this method also facilitates the study of protonated species [67]. As an example, the production of cationic and protonated benzoic acid by charge transfer from its ionic UV photolysis products is shown in Fig. 2.

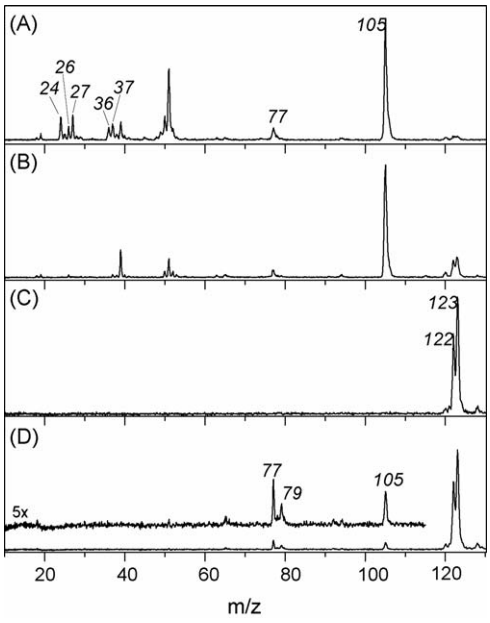


Fig. 2. Mass spectra during the experimental sequence used to record the IR spectrum of the benzoic acid cation [67]. The ArF laser pulse does not create cationic benzoic acid but only cationic benzoyl, $C_6H_5CO^+$ ($m = 105$) and smaller photolysis products such as $C_2^+$, $C_2H_2^+$, $C_2H_3^+$, $C_3^+$, and $C_3H^+$ (A). The high IP of these small fragments drives the charge transfer to neutral benzoic acid ($m = 122$) as observed in the mass spectrum taken after a reaction delay of about 200 ms (B). In addition, proton transfer produces protonated benzoic acid. Temporarily raising the RF amplitude isolates the parent ions (C) and subsequent irradiation with the FEL at about 1175 $cm^{-1}$ induces dissociation (D). The benzoic acid cation fragments by loss of OH to mass 105 and by loss of CO and OH to mass 77, whereas protonated benzoic acid dissociates by loss of $CO_2$ to protonated benzene ($m = 79$).

### 2.2. Computational

In order to interpret the experimental infrared spectra, comparison was made to results from density functional theory (DFT) calculations. Unless otherwise stated, geometry optimization and harmonic frequency calculations are carried out with the Becke3LYP hybrid functional [70,71] and the double-zeta D95(d,p) basis set using the Gaussian98 software package [72]. This level of theory is found to adequately describe the geometries as well as the vibrational spectra of these types of ions [73–76]. It should be noted that the resulting infrared spectrum represents a linear absorption spectrum, which may differ from the experimentally obtained IRMPD spectrum. Effects of the multiple photon excitation mechanism on the appearance of the spectrum are described in the following sections.

## 3. IR spectra of cationic PAHs

Our experiments [45,76–78] have mainly focused on the mid-infrared spectroscopy of cationic polycyclic aromatic hydrocarbons (PAHs) because of their hypothesized abundance in inter- and circumstellar environments. Based on the observation of very similar infrared emission spectra from a large variety of inter- and circumstellar clouds, PAH molecules and ions were hypothesized to be abundantly present in these clouds [79–84]. These molecules are suggested to be excited by stellar UV radiation and to undergo internal conversion, giving rise to vibrational excitation in the molecules. Due to the lack of collisions in low-density interstellar environments, the molecules cool via infrared emission [85,86]. Depending mainly on the ratio of the local UV flux and electron density [87], the molecules may occur in their ionized state(s), and particularly in the vicinity of stars, the fraction of cationized PAHs may be substantial [88,89]. The main

body of laboratory infrared data on cationized PAH molecules relies on matrix isolation spectroscopy [90–94], which suffers from the inherent possibility of unknown interactions between the matrix and the molecules under study [95]. Some IR spectra of PAH cations obtained via emission spectroscopy [83] as well as via molecular beam IR-UV double resonance methods [96,97] have been reported as well. We applied a FEL-based method to collect IRMPD spectra for a number of cationic PAHs in the gas phase [45,77,76,78].

An overview of our studies in an astrophysical perspective is given in Ref. [98], and here, we will give an overview of the spectroscopic analyses. We discuss several interesting aspects of the $PAH^+$ IR spectra in comparison with the DFT computations, and then briefly discuss the effects of vibronic interaction in radical PAH cations with high symmetry.

### 3.1. Comparison with DFT

The IRMPD spectra for 12 cationic PAH molecules ranging in size from naphthalene to coronene are shown in Fig. 3. Interestingly, we were unable to obtain spectra for smaller (unsubstituted) aromatics, most notably for the benzene cation [99–101]. This is possibly due to the small size and the inherent low density of states, which prevented us from overcoming the anharmonicity bottleneck (see Section 4.1). The experimental spectra in Fig. 3 are compared to the results from DFT calculations, convoluted with a 30 $cm^{-1}$ FWHM Gaussian line profile. DFT calculated harmonic frequencies were uniformly scaled with a factor of 0.96 to account for anharmonicity as well as for experimental redshifting of bands caused by multiple photon excitation.

The general features of PAH infrared spectra are well known and are also recognized in our spectra. To the red, typically around 700–800 $cm^{-1}$, the CH out-of-plane bending modes are found. The exact position of the band is dependent on the number of neighbouring CH units on an aromatic ring [102]. The spectral range between 1000 and 1600 $cm^{-1}$ contains delocalized vibrational modes of CH in-plane bending and CC stretching character, with the latter usually located more to the blue end of the range. As compared to neutral PAHs, these modes gain up to a factor of 10 in intensity, making them the strongest bands in the spectra [103]. In contrast, the CH stretch modes around 3 μm, which are not covered in our spectra, are known to decrease drastically in intensity, compared to the neutral species.

For most species, a reasonably good correspondence between experiment and theory is found. However, several discrepancies are also apparent in Fig. 3, and the most striking ones are further discussed here.

The experimental spectrum of the phenanthrene cation ($C_{14}H_{10}^+$, Fig. 3B) deviates slightly from the theoretical spectrum in the range between 900 and 1200 $cm^{-1}$. These discrepancies were studied at improved spectral resolution in a molecular beam by Piest et al. [97]. The matrix isolation spectrum of cationic phenanthrene shows a similar deviation from theory. A low-lying electronically excited state, not accounted for in the DFT calculation, was speculated to cause these deviations [97].

The experimental spectrum of the fluorene cation ($C_{13}H_{10}^+$, Fig. 3D) is in reasonable agreement with the theoretical spectrum except for one band near 1060 $cm^{-1}$, which is not reproduced by the calculation [76]. It is known that the fluorene molecule easily looses an H-atom from the aliphatic $CH_2$ group upon non-resonant ionization. The bond dissociation energy is estimated to be around 2 eV [104,105]. In the ion trap experiments, the fluorene cation at $m/z = 166$ and the dehydrogenated cation at $m/z = 165$ could not be resolved. The spectrum computed for this fragment ion is very similar to that computed for the fluorene radical cation, except that it shows additional intensity around 1050 $cm^{-1}$, which could therefore explain the discrepancies observed in Fig. 3D [76]. Observation of the fluorene cation infrared spectrum in a high-resolution mass spectrometer definitively proved the spurious band to be not due to the fluorene cation [106].

A similar effect is likely responsible for the main discrepancies between the experimental and theoretical spectra of the benzofluorene cation ($C_{17}H_{12}^+$, Fig. 3E). As for the fluorene cation, one of the hydrogen atoms on the aliphatic $CH_2$ group is easily detached, forming a closed-shell $C_{17}H_{11}^+$ cation [107]. The DFT computed spectrum of the dehydrogenated benzofluorene cation (not shown) features additional infrared bands at 510 and 1087 $cm^{-1}$, close to the additional bands in the observed spectrum.

Pronounced discrepancies between experiment and theory are observed for the fluoranthene cation ($C_{17}H_{12}^+$, Fig. 3F). The B3LYP calculated spectrum of the $C_{2v}$ optimized structure contains one imaginary frequency, which points in the direction of a distortion to a $C_s$ structure. This problem was already encountered in the analysis of the matrix isolation spectrum of the fluoranthene cation [94]. Bauschlicher et al. [75] explained this symmetry breaking in terms of a mixing of the singly occupied and highest doubly occupied molecular orbitals. When using the BP86 functional, no symmetry breaking is observed and the minimum energy structure has $C_{2v}$ symmetry [75]. The corresponding spectrum is in better agreement with the experiment (see Fig. 4).

The triphenylene cation ($C_{18}H_{12}^+$, Fig. 3K) infrared spectrum shows substantial deviations from the computed spectrum, which are not fully understood. The problems are possibly due to Jahn-Teller distortion of the triphenylene cation, as discussed in the following section.

Depending on the level of detail that one considers, more discrepancies can be found and it is not possible to find an explanation for every single one of them. These deviations may be due to experimental effects, such as in the case of the fluorene cation, as well as to computational effects, as in the case of the fluoranthene cation. Nonetheless, despite these discrepancies for individual species, the general agreement between the experimental IRMPD spectra and the DFT computed linear absorption spectra is reasonably good. In fact, this is quite surprising since the MPD process requires the absorption of on the order of 100 infrared photons by a single molecule. In chapter 4 we present a detailed discussion of the multiple photon excitation process, and describe a mathematical model to simulate the IRMPD spectra.

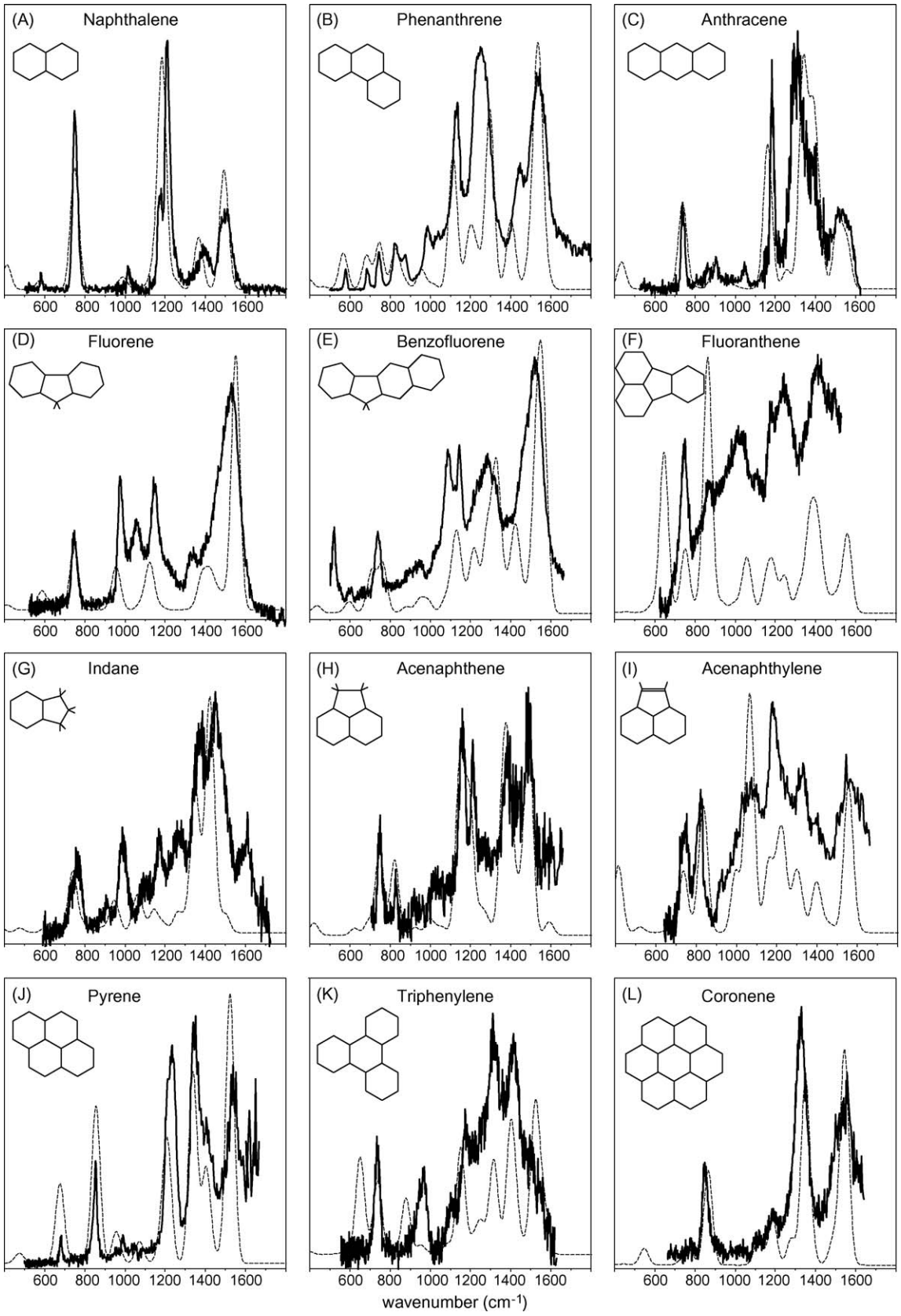


Fig. 3. IRMPD spectra (thick line) of 12 cationic PAH species compared to DFT frequency calculations (thin line) convoluted with a 30 $cm^{-1}$ FWHM Gaussian band profile.

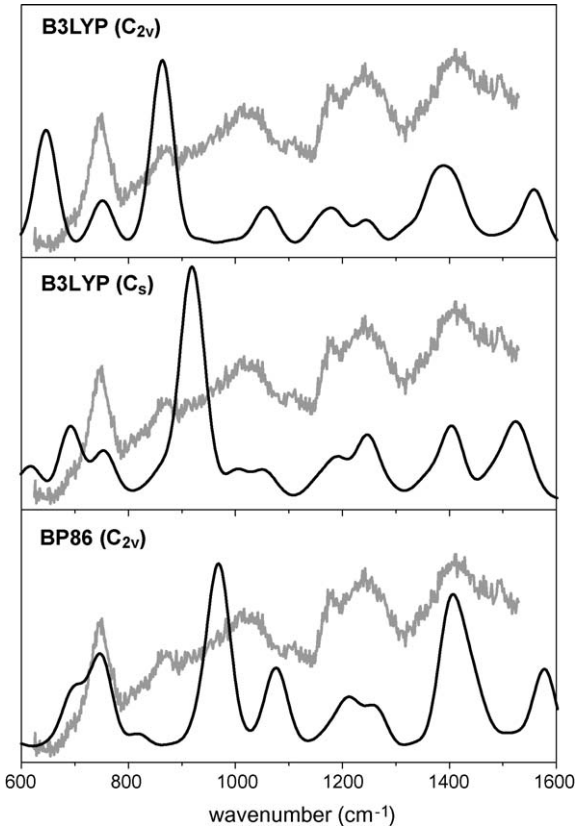


Fig. 4. IRMPD spectrum (light) of the fluoranthene cation compared to B3LYP calculations (dark) at the $C_{2v}$ saddle point structure, the $C_s$ minimum structure and to a BP86 calculation, which predicts the $C_{2v}$ structure to be the global minimum.

### 3.2. Vibronic interaction

The Jahn-Teller theorem states that a radical species in a degenerate electronic state is subject to a vibronic interaction that forms a conical intersection at the symmetric geometry, causing the molecule to distort to a lower symmetry structure [108–111]. The reduction of symmetry lifts the degeneracy of the singly occupied molecular orbital and lowers the overall energy of the system. To possess degenerate irreducible representations, a molecule must possess a three-fold or higher symmetry axis. Therefore, in the set of radical PAH cations studied here, coronene and triphenylene are susceptible to Jahn-Teller interaction. We have not pursued a full Jahn-Teller analysis of these spectra, but have instead analyzed the distorted structures and their harmonic frequencies with DFT. Two distorted geometries having lower symmetry and non-degenerate HOMOs were optimized with DFT. For the cationic PAHs considered here, the difference in energy between the distorted structures is very small so that they are likely to 'psuedo-rotate' in the potential moat formed around the conical intersection [111]. The time-averaged, or dynamical, structure is then similar to the non-distorted symmetrical structure, as is for instance the case in cationic benzene [110,112].

The neutral coronene molecule has $D_{6h}$ symmetry and has a degenerate highest occupied molecular orbital (HOMO) of $e_{2u}$ symmetry [113]. Upon ionization, an electron is removed from one of the degenerate HOMOs, and the ion Jahn-Teller distorts to a $D_{2h}$ geometry. Two distinct $D_{2h}$ structures can be formed by either stretching or compressing the geometry. One of the two structures forms the potential minimum, while the other forms a saddle point structure. The infrared spectrum calculated at the minimum energy $D_{2h}$ structure agrees well with the observed IRMPD spectrum, as can be seen in Fig. 3L.

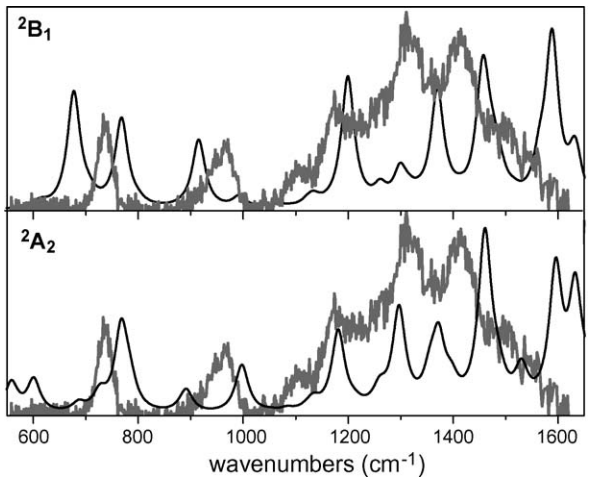


Fig. 5. IRMPD spectrum of cationic triphenylene compared with B3LYP/D95(d,p) calculated spectra for the two structures distorted to $C_{2v}$ symmetry: the $^2B_1$ minimum energy structure and the $^2A_2$ saddle point structure.

A similar approach was used for the triphenylene cation. The corresponding neutral molecule has $D_{3h}$ symmetry and an $e''$ degenerate HOMO [114,115]. In the cation, Jahn-Teller distortion causes symmetry lowering to $C_{2v}$ and two electronic states result. Geometry optimization in $C_{2v}$ yielded a $^2B_1$ ground state structure. A $^2A_2$ state is found to be a transition state, although the difference in energy is only 7.6 cm$^{-1}$ at the B3LYP/D95(d,p) level of theory. Note also that this difference is so small that the states were seen to reverse depending on the computational method used [114]. Unlike the coronene cation, the calculated infrared spectrum for the minimum energy $^2B_1$ structure does not give a satisfactory match with the experimental spectrum, as is obvious from Fig. 3K. In a computational study [73], Langhoff published a similar infrared spectrum for cationic triphenylene, which emphasizes the difficulties with this type of systems. Interestingly, the spectrum calculated at the $^2A_2$ saddle point structure appears to show slightly better agreement (see Fig. 5). A recent calculation [115] shows that the vibronic coupling is particularly strong for the $E'$ vibrational modes of CC stretching character around 1600 cm$^{-1}$ and of CH out-of-plane bending character around 800 cm$^{-1}$.

## 4. Dynamics of IRMPD

The interpretation of IRMPD spectra is generally done by comparison to spectra calculated using quantum chemical methods (see above), which obviously yield linear absorption spectra. Since the IRMPD process involves the absorption of multiple, even up to hundreds of, photons, it is interesting to evaluate at

least qualitatively the effects of multiple photon excitation on the infrared spectrum.

### 4.1. Multiple photon excitation in polyatomic molecules

First of all, it is good to recall that all molecular vibrations are anharmonic to some extent, which generally causes the spacing of the levels to become smaller as one climbs up the vibrational energy ladder of a vibrational mode. One should also appreciate that dissociation thresholds for typical (ionic) polyaromatic molecules are on the order of 6–8 eV so that at least 60 photons at a wavelength of 10 μm need to be absorbed for fragmentation to occur. Therefore, coherent multiphoton excitation, where all photons are absorbed in one vibrational ladder in a stepwise process ($v_i = 0 \rightarrow v_i = 1 \rightarrow v_i = 2 \rightarrow \cdots$), is unrealistic at moderate laser intensities and this effect is often referred to as the *anharmonicity bottleneck* [12,18].

However, in polyatomic molecules, such as the polyaromatics mainly investigated here, the interaction of laser radiation with the molecule leads to incoherent multiple photon excitation. Note that we will use the terminology of [116,117], where these non-coherent processes are referred to as *multiple photon* excitation, in contrast to coherent *multiphoton* excitation. Rather than coherent ladder climbing within one vibrational mode, the energy of each photon absorbed diffuses, due to anharmonic coupling between vibrational modes, over the bath of vibrational background states of the molecule. This process is commonly referred to as intramolecular vibrational redistribution (IVR) [118]. When the molecule is large enough, i.e., the density of states is large enough, IVR rapidly removes the population from the excited state into the bath of vibrational background states so that the molecule is ready for the next photon absorption. The short vibrational lifetimes induced by IVR result in a broadening of absorption lines.

At room temperature, IVR lifetimes of aromatic molecules are typically much less than 1 ns [119,120]. Although the IVR rate is not directly determined by the density of states ($\rho$) (as was shown by different high-resolution experiments on the CH stretching modes of several hydrocarbon molecules), but by the presence of low-order coupled *doorway states* and the magnitude of the coupling matrix elements [118], it defines the statistical limit and thus the degree of irreversibility of vibrational energy diffusion [121]. For the polyaromatic molecules investigated here it appears safe to assume an IVR lifetime of $<1$ ns, which corresponds to the micropulse spacing of FELIX. Thus, the excited vibrational mode is de-excited through "dissipation" of the energy into the bath of states by the time the next micropulse arrives.

This process of incoherent multiple photon excitation is often described in terms of a *quasi-continuum* of vibrational states occurring at high internal energies [12,116,117]. Although the name quasi-continuum suggests that photons of any wavelength can be absorbed, this region is characterized by semi-resonant absorption in zones near the original fundamental transition [12,122]. These zones represent the background vibrational states that borrow intensity from the bright state via (indirect) anharmonic coupling. The spectral width ($\Gamma$) of these zones is determined by Fermi's Golden Rule $\Gamma = 2\pi\langle W^2\rangle\rho$, in which the mean squared coupling matrix element $\langle W^2\rangle$ is dominated by the strongly coupled doorway states, the first tier of coupled states. From this equation, one can also immediately see that increasing the density of states does not necessarily increase the linewidth, if the additional states couple only very weakly to the bright state [118].

The criterion of stochasticity [12,18] defines the onset of the quasi-continuum as the internal energy where

$$2\pi c\tau_{\mathrm{IVR}} = \rho(E) \tag{1}$$

In other words, in the quasi-continuum, the IVR lifetime broadening exceeds the average mode spacing. Assuming an IVR lifetime of $\leq$1 ns, the coronene cation already finds itself in the quasi-continuum at thermal energies. For the naphthalene ion, this boundary is reached already after the absorption of one photon at say 1000 $\mathrm{cm}^{-1}$. Most photons are therefore absorbed while the molecules reside in the quasi-continuum of vibrational states. Nevertheless, well-resolved spectra are generally observed, in agreement with the existence of narrow semi-resonant zones.

### 4.2. Mathematical model

To obtain better insight into the IRMPD process, a mathematical model based on coupled rate equations describing the population in the energy levels involved was developed. We briefly discuss the methods used to determine the density of states and the general background of the model, and then sketch its mathematical implementation. Sections 4.2–4.4 discuss experimental manifestations of the multiple photon excitation process, that are (partly) explained in terms of this model.

#### 4.2.1. Determination of the density of states

Usually the region of very low vibrational energies is out of practical interest in the case of large polyatomic molecules. The density of vibrational states in the region of the quasi-continuum can be estimated by using the quasi-classical approximation for the density of vibrational states [109]

$$\rho(E) = \frac{1}{(s-1)!}\frac{E^{s-1}}{\prod_{i=1}^{s}\hbar\omega_i}, \tag{2}$$

where $s$ is the number of vibrational degrees of freedom of the molecule, $E$ the vibrational energy and $\omega_i$ is the frequency of the $i$th vibrational mode. The validity of the quasi-classical formula is justified only for very high vibrational quantum numbers $v_i$ and thus for vibrational energies $E \gg \sum_i \hbar\omega_i$. A better description can be obtained with a correction to the quasi-classical formula as given by [123]

$$\rho(E) = \frac{1}{\hbar\omega_m}\frac{\Gamma(E/\hbar\omega_m + s)}{(s-1)!\,\Gamma(E/\hbar\omega_m + 1)} \tag{3}$$

where $\omega_m = \sqrt[s]{\prod_{i=1}^{s}\omega_i}$ is the geometric mean of the vibrational frequencies.

Instead of using an analytical desription of the density of vibrational states, accurate counting algorithms exist that allow

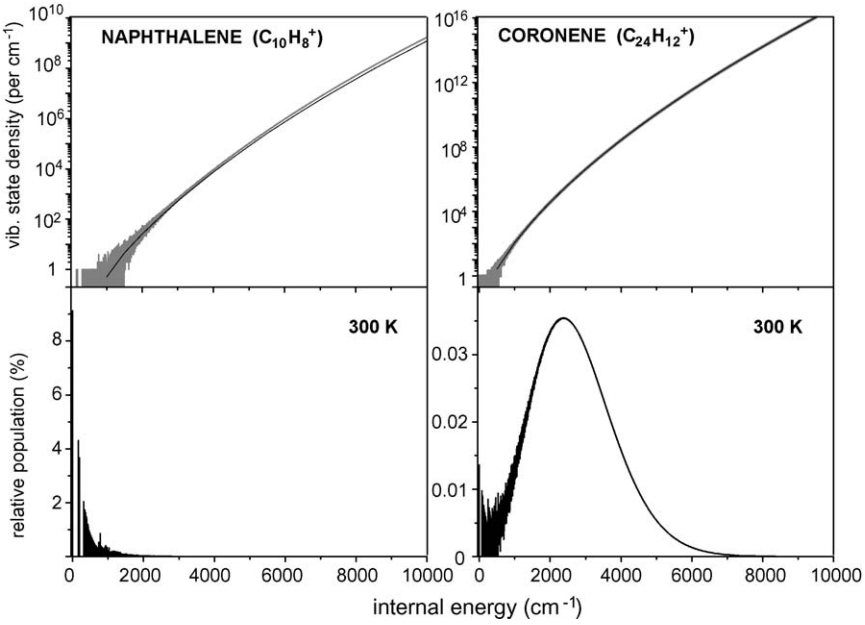


Fig. 6. Vibrational state densities for the smallest and largest PAH cations studied in this work, naphthalene and coronene (upper panels), calculated using the Beyer-Swinehart direct counting algorithm (gray) and the corrected quasi-classical approach (black). Assuming a Boltzmann distribution at room temperature, the relative populations in the vibrational levels is calculated (lower panels), which shows for instance that only 9% of the naphthalene cations are in the vibrational ground state. For the coronene ion this fraction is on the order of 0.01%.

the state density to be numerically evaluated. For instance, the Beyer-Swinehart algorithm [124] is well known as an efficient method to determine the state density, with as input the fundamental vibrational frequencies of the molecule. An advantage of these methods is that they account directly for the discontinuous behaviour of the state density at low internal energies. As an example, in Fig. 6 the density of vibrational states is calculated for the naphthalene and coronene cations using the Beyer-Swinehart algorithm and the DFT calculated harmonic frequencies. The density of states calculated using the corrected quasi-classical approximation of Eq. (3) is also plotted and it can be seen to give a good estimate of the density of states, even for low internal energies.

The lower panels in Fig. 6 show the vibrational state distributions assuming a Boltzmann distribution at room temperature. From these distributions the average internal energy at room temperature is determined as 1017 and 2724 cm$^{-1}$ for the naphthalene and coronene cations, respectively. Although the density of vibrational states of the naphthalene cation is still relatively low, single digit, at room temperature, that of the coronene molecule amounts already to $10^4 - 10^5$ vibrational states per cm$^{-1}$.

### 4.2.2. The statistical model in a high density vibrational spectrum

Based upon Fermi's Golden Rule, the IR induced dipole moment transition rate $E' \leftarrow E$ for one photon absorption or emission between levels in a dense vibrational spectrum, can be calculated as

$$k_{E'\leftarrow E} = \frac{\pi}{2\hbar}\mathbf{E}_0^2 \cos^2\theta\,|\mu_{E',E}|^2\rho(E') \tag{4}$$

where $\hbar\omega = |E - E'|$ is the photon energy, $\mu_{E',E} = \langle E'|\mu|E\rangle$ is the dipole moment matrix element, $\mathbf{E}_0$ the amplitude of the monochromatic laser field $\mathbf{E} = 1/2\mathbf{E}_0(e^{i\omega t} + e^{-i\omega t})$, and $\theta$ the angle between the laser polarization and the transition dipole moment. The absorption cross-section can be related to the transition rate via $k = \sigma I/\hbar\omega$, where $I$ is the intensity of the laser field given by $I = c\,\mathbf{E}_0^2/8\pi$. Assuming the laser polarization to be linear with a mean orientation $\overline{\cos^2(\theta)} = 1/3$, the cross-section reads

$$\sigma_{E'\leftarrow E} = \frac{4\pi^2}{3c}\,\omega\,|\mu_{E',E}|^2\,\rho(E') \tag{5}$$

providing the detailed balance relationship: $\sigma_{E'\leftarrow E}/\sigma_{E'\rightarrow E} = \rho(E')/\rho(E)$.

Calculation of the matrix elements $\mu_{E',E}$ within a dense vibrational spectrum is not trivial because the actual eigenstates must be determined taking into account the anharmonic part of the vibrational Hamiltonian. Although the anharmonic part of the potential is much smaller than the harmonic part, anharmonicity can result in heavy mixing of harmonic eigenstates because of the extremely high density of vibrational states. Unfortunately, anharmonicity parameters of polyatomic molecules are rarely known and even if they would be known, a general theory of eigenstates of a multidimensional anharmonic oscillator has not yet been elaborated.

The power expansion of the dipole moment operator

$$\mu = \mu_p + \sum_i \frac{\partial\mu}{\partial Q_i}Q_i + \frac{1}{2}\sum_{i,j}\frac{\partial^2\mu}{\partial Q_i\partial Q_j}Q_iQ_j + \cdots \tag{6}$$

can be used to calculate the dipole moment matrix elements in Eq. (5). The permanent dipole moment $\mu_p$ is not relevant for IR excitation and only the linear terms are considered because of the small vibrational amplitudes.

The vibrational coordinate of $i$th mode, $Q_i$, can be expressed in terms of the annihilation and creation operators as $Q_i = \sqrt{\hbar/2m_i\omega_i}(a_i^\dagger + a_i)$ [125]. Since the matrix elements of annihilation and creation operators in the basis set of the harmonic oscillator are $\langle v_i'|a_i^\dagger|v_i\rangle = \delta(v_i', v_i+1)\sqrt{v_i+1}$ and $\langle v_i'|a_i|v_i\rangle = \delta(v_i', v_i-1)\sqrt{v_i}$, the dipole moment matrix elements of up-transitions ($E' > E$) can be expressed as

$$\mu_{E',E} \simeq \sum_i \frac{\partial\mu}{\partial Q_i}\sqrt{\frac{\hbar}{2m_i\omega_i}}\langle E'|a_i^\dagger|E\rangle \simeq \frac{\partial\mu}{\partial Q_i}\sqrt{\frac{\hbar}{2m_i\omega_i}}\langle E'|a_i^\dagger|E\rangle. \quad (7)$$

The "narrow-band simplification" obtained by omitting all terms except the $i$th term from the sum is rationalized by the fact that even in the region of a high state density, the anharmonic part of the Hamiltonian is smaller than the harmonic part, and hence the matrix elements $\langle E'|a_i^\dagger|E\rangle$ must obey the narrow resonance condition $\omega \sim \omega_i \pm \delta E_{\text{anh}}/\hbar$, where $\delta E_{\text{anh}}$ is the shift from resonance due to anharmonicity and the IVR induced broadening in the region of the $i$th mode. Outside these narrow absorption zones within the quasi-continuum, matrix elements are assumed to be negligible, which will be justified by comparison with experimental IRMPD spectra.

The absorption cross-section at an excitation frequency $\omega \approx \omega_i$ can now be expressed as

$$\sigma_{E'\leftarrow E} = A_{01(i)}|\langle E'|a_i^\dagger|E\rangle|^2\rho(E') \quad (8)$$

where $A_{01(i)} = (4\pi^2/3c)\omega|\mu_{01(i)}|^2$ is the integral absorption cross-section and $\mu_{01(i)} = (\partial\mu/\partial Q_i)\sqrt{\hbar/2m_i\omega_i}$ is the dipole moment of the fundamental $v_i = 0 \rightarrow 1$ transition. For dense vibrational spectra with heavy mixing of harmonic states due to anharmonicity, it is hard to calculate the matrix elements $\langle E'|a_i^\dagger|E\rangle$. However, the matrix element $|\langle E'|a_i^\dagger|E\rangle|^2$ has the integral property [125]

$$\int_{E'\sim E+\hbar\omega_i} |\langle E'|a_i^\dagger|E\rangle|^2\rho(E')\mathrm{d}E' = \int_{E'\sim E+\hbar\omega_i} \langle E|a_i|E'\rangle\rho(E')\langle E'|a_i^\dagger|E\rangle\,\mathrm{d}E' = \langle E|a_i a_i^\dagger|E\rangle = 1 + \langle E|\hat{v}_i|E\rangle \quad (9)$$

where $\hat{v}_i = a_i^\dagger a_i$ is the vibrational number operator [125]. It is reasonable to introduce the following factorization

$$|\langle E'|a_i^\dagger|E\rangle|^2 = \hbar f_i(\omega-\omega_i, E)(1+\bar{v}_i(E)) \quad (10)$$

where $f_i(\omega-\omega_i, E)$ is the form factor of the transition $E \rightarrow E' = E + \hbar\omega$, which has a resonance shape near $\omega_i$ and $\bar{v}_i(E)$ is the mean number of quanta in the $i$th mode. When IVR is faster than the IR photon absorption rate, $\bar{v}_i(E)$ can be replaced by its statistically averaged value for a given vibrational energy $E$. Calculation of the actual form factor $f_i(\omega-\omega_i, E)$ is impractical and we shall model its shape with well known line shape functions.

*4.2.3. Implementation of the model*

The dynamics of the population distribution in the ladder of resonant vibrational levels $E_0, E_0+\hbar\omega, \cdots, E_m = E_0 + m\hbar\omega, \cdots$ pumped by a laser field of frequency $\omega$ can be described by the kinetic equations [126]

$$\mathrm{d}n_m/\mathrm{d}t = k_{m+1,m}n_{m+1} + k_{m-1,m}n_{m-1} - k_{m,m+1}n_m - k_{m,m-1}n_m \quad (11)$$

where $n_m$ is the population of the $m$th level and the rates of the laser induced transition $E_i \rightarrow E_j$ are defined according to Eqs. (4) and (5) as $k_{i,j} = (I/\hbar\omega)\sigma_{i,j}$. The cross-sections of up and down transitions satisfy the detailed balance principle $\sigma_{m,m+1}/\sigma_{m+1,m} = \rho(E_{m+1})/\rho(E_m)$.

The absorption cross-section $\sigma_{m,m+1}(\omega, E)$ depends sensitively on the laser frequency $\omega$ due to the sharp resonance condition. The width of the resonances is much smaller than the vibrational frequencies since the IVR rates determining the linewidth are of the order of the vibrational anharmonicities, which are much smaller than the vibrational frequencies. Using Eqs. (8)–(10), the absorption cross-section in the vicinity of the $i$th vibrational mode can be expressed as

$$\sigma_{m,m+1}(\omega, E) = A_{0,1(i)}f_i(\omega-\omega_i, E)(1+\bar{v}_i(E)/d_i) \quad (12)$$

where $A_{0,1(i)}$ is the integral absorption cross-section of the $i$th fundamental transition, $\bar{v}_i(E)$ the statistically averaged number of quanta in the $i$th vibrational mode at energy $E$, $d_i$ the degeneracy of the $i$th mode, and $f_i(\omega-\omega_i, E)$ is the normalized resonance form factor.

To calculate the average number of quanta in the $i$th mode, the molecule with vibrational energy $E$ is treated as a thermodynamical ensemble of vibrational oscillators at an effective temperature $T$, so that

$$E = \sum_i \frac{d_i\hbar\omega_i}{\exp(\hbar\omega_i/kT)-1} \quad (13)$$

The average number of quanta in the $i$th mode is then determined as

$$\bar{v}_i(E) = \frac{d_i}{\exp(\hbar\omega_i/kT)-1} \quad (14)$$

The resonance form factor is modelled with a normalized Lorentzian function

$$f_i(\omega-\omega_i, E) = \frac{\Gamma_i(E)}{\pi[(\omega-\omega_i-\delta\omega_i(E))^2 + (\Gamma_i(E))^2]} \quad (15)$$

We assume that both the width of the Lorentzian, $\Gamma_i(E)$, and the deviation $\delta\omega_i(E)$ of the resonant frequency from its harmonic value $\omega_i$ originate from the anharmonicity of the vibrations, which can be considered as a small perturbation of the harmonic Hamiltonian. Thus, to first order, both parameters can be approximated as being linearly dependent on excitation energy $E_m = m\hbar\omega$ [126]

$$\Gamma_i(E_m) = b_i m, \qquad \delta\omega_i(E_m) = -a_i m. \quad (16)$$

The expression for $\sigma_{i,j}$ is further convoluted with the spectral profile of the laser radiation, which is assumed to be Lorentzian as well. The contribution of the rotational contour to the form

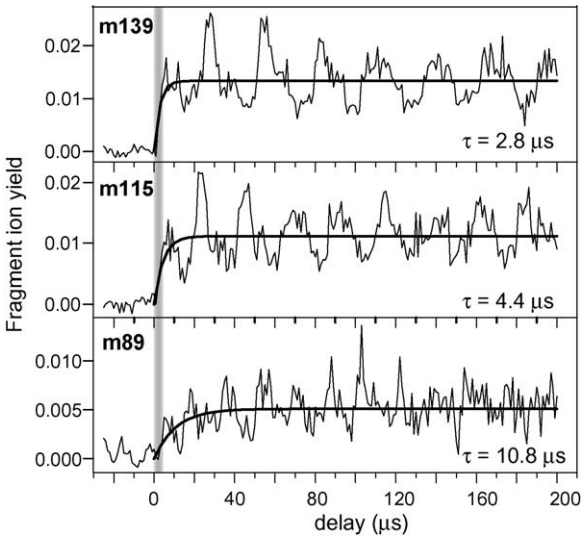


Fig. 7. Dissociation yield at ≈1540 cm$^{-1}$ as a function of time delay between the FELIX pulse, indicated by the shaded area at $t = 0$, and ion extraction from the trap into the TOF-MS, for three different fragment channels observed upon multiple photon dissociation of the fluorene cation. The fitted curves clearly indicate how the dissociation rate slows down for the higher energy channels (leading to lower mass fragments).

factor was neglected because of the small rotational constants of the polyaromatic molecules studied here.[1]

Where available, $a$ and $b$ parameters were estimated from temperature dependent emission studies on gas-phase molecules and then fitted when simulating the experimental IRMPD spectra. Values for the integral absorption cross-sections as well as for harmonic vibrational frequencies were taken from DFT calculations. The initial population distribution over the vibrational levels was assumed to be thermal: $n(E) = \rho(E)\ \exp(-E/kT)/Z$, where $Z$ is the partition function (see Fig. 6).

### 4.3. Time-resolved dissociation

Before embarking on applying these mathematical methods to model spectral characteristics of IRMPD spectra, it is interesting to look at the infrared induced dissociation in a time-resolved fashion. Assuming statistical behavior, the rate of dissociation is directly related to dissociation threshold. To observe the rate of dissociation, the fragmentation of the fluorene cation into different dissociation channels is recorded as a function of the time delay between the FEL pulse and the extraction of the ions from the trap. Fig. 7 shows the fragment intensities on the m139, m115, and m89 fragments from fluorene (m166) for time delays between −20 and 200 μs.

One may note here that (some of) the observed fragmentation channels may be due to sequential absorption/dissociation/absorption/dissociation processes, in which the infrared induced fragment ions absorb additional photons to undergo subsequent dissociation processes. In that case, the picture would be more complicated than the simple picture of unimolecular decay. In the next section, we unambiguously show that direct dissociation into higher energy exit channels can be induced at the pulse energy levels provided by the FEL. However, the possibility of sequential processes cannot be excluded here, but it is only of minor relevance for the qualitative arguments presented in this section.

Inspecting Fig. 7, we first note that the intensity oscillations at a frequency inversely proportional to the mass of the fragment, can be attributed to the secular motion of the ions in the trap [127]. Since the period of the secular motion is substantially longer than the FEL pulse, a coherence in the secular motion is induced, which leads to a "breathing" motion of the ion cloud. Since sampling of the ion cloud proceeds through a small hole in one of the endcaps, this breathing motion causes a modulation of the amount of ions that is actually extracted from the trap. This effect can be reduced by increasing the size of the extraction hole in the endcap [128]. In the following, we shall simply ignore the secular motion induced oscillations.

A simple exponential fit of the onset of dissociation after the laser pulse, shown in Fig. 7, gives an estimate of the dissociation rates of $3.6 \times 10^5$, $2.3 \times 10^5$, and $9.3 \times 10^4$ s$^{-1}$ for the mass channels 139, 115, and 89, respectively. Although the dissociation pathways of the fluorene cation have been studied in detail [104,105], thresholds for the different fragment channels are not accurately known. However, for this ion it is reasonable to assume that the activation energies are higher for the production of lower mass fragment ions, as their generation requires (more) rearrangement. The observed decreasing rate of dissociation with lower mass fragment channels is then at least in qualitative agreement with that assumption.

It is now tempting to quantify the internal energy of the ions reached in the excitation process based upon the observed dissociation rates. However, not only are the dissociation thresholds for the different channels unknown, a more fundamental difficulty is, that after IR excitation, not all ions will have the same internal energy. Moreover, there is no reason to assume that one has a distribution that resembles a thermal distribution. In a zeroth order picture, a Poisson distribution might be more appropriate. More rigorous estimates show that the distribution can have a highly irregular shape. We illustrate this by analyzing the IRMPD spectrum of the coronene cation.

### 4.4. Effects of multiple photon excitation on the appearance of the spectrum

A calculation of the IRMPD spectrum of a molecule requires knowledge of its anharmonic parameters. Although the anharmonicity of individual vibrational modes, i.e., the self-anharmonicity, can be calculated, what is needed really is the average cross-anharmonicity of a mode with all other modes. In practice, it requires the knowledge of the shift of each vibrational mode with internal energy. It is possible to experimentally determine these parameters by measuring the shift of vibrational modes as a function of the temperature of the sample. Such experiments were carried out for several neutral PAHs, including coronene, by Joblin et al. [129].

[1] Typically on the order of a few hundredths of a wavenumber, which would give rotational contours of only a few cm$^{-1}$ at room temperature.

The values for the temperature dependent broadening and shifting of vibrational bands for neutral coronene as reported in Ref. [129] were assumed to be similar for the corresponding modes in the cation. The $\chi'$ and $\chi''$ parameters of Ref. [129], describing the shift and broadening as a function of temperature, can be converted to the $a$ and $b$ parameters of Eq. (16) via

$$a_i = \chi_i' \hbar\omega_i \left[\frac{\mathrm{d}E(T)}{\mathrm{d}T}\right]^{-1}, \qquad b_i = \chi_i'' \hbar\omega_i \left[\frac{\mathrm{d}E(T)}{\mathrm{d}T}\right]^{-1} \tag{17}$$

The scaled DFT calculated frequencies were used as the zero-temperature band positions. Further, the laser fluence was estimated as $20\,\mathrm{J\,cm^{-2}}$ and a laser bandwidth of $4\,\mathrm{cm^{-1}}$ was assumed. Using these values and our model results in a multiple photon excitation spectrum as plotted in the upper panel of Fig. 8. The curve represents the average internal energy, which is obtained from the internal energy distribution calculated at each excitation wavelength.

Let's consider the three wavelengths indicated with an arrow. Excitation at these wavelength leads to similar *average* internal energies, however, the corresponding internal energy *distributions*, shown in the three insets, are quite distinct. The gray shaded area in the insets indicates the dissociation rate, being $10^4\,\mathrm{s^{-1}}$ at an energy of about 12 eV [130]. Clearly, these distributions can be quite oddly shaped, and this can have consequences for the dissociation yield. For instance, the distribution calculated for an excitation photon energy of $1136\,\mathrm{cm^{-1}}$, has a double peak shape. This is due to the proximity of another absorption band at slightly higher energies, which upon excitation, i.e., upon increasing internal energy, shifts into resonance with the laser radiation as a consequence of anharmonicity. This effect occurs only for the high energy tail of the distribution, which therefore undergoes a second boost of energy. The result is that the three bands indicated with arrows show a significant difference in calculated dissociation yield, whereas their average internal energies are quite similar. From a comparison with the experimental spectrum, it may be concluded that such effects are very difficult to model accurately. It should however be noted that no anharmonic parameters are available for these low intensity bands from Ref. [129] and therefore, average values were used for these modes. The main bands in the spectrum appear to be well reproduced by the model calculation.

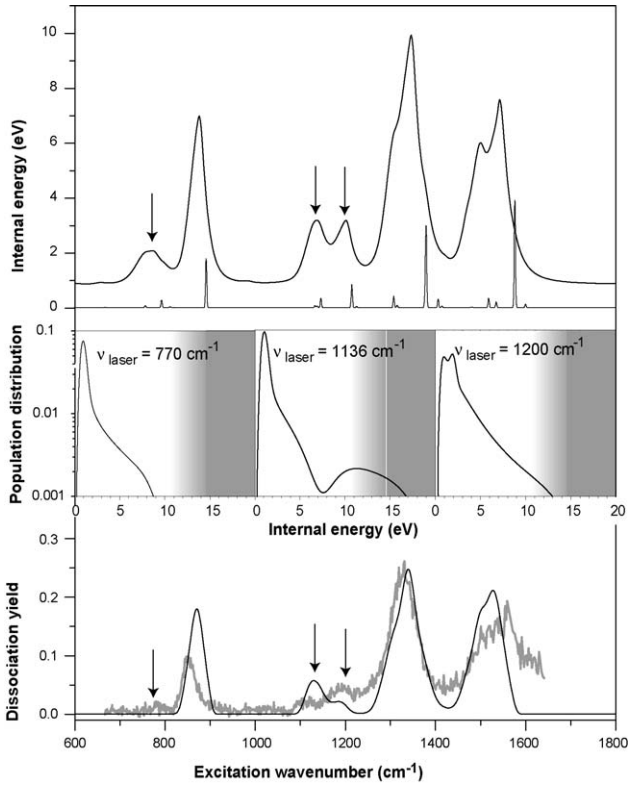


Fig. 8. Calculated average internal energy reached versus excitation wavenumber for the coronene cation (upper panel). The DFT computed spectrum is indicated with the thin line. The actual internal energy distributions at three different laser wavelengths are plotted in the insets, where the gray shaded area indicates the dissociation threshold. The lower panel shows the wavelength dependent dissociation yield obtained, compared to the observed IRMPD spectrum in gray. Note that the three bands which give rise to an approximately equal average internal energy do not necessarily give rise to the same dissociation yield since the internal energy distributions are quite different.

### 4.5. Competing fragmentation channels: effects on the spectrum

As a consequence of the anharmonicity, absorption frequencies shift to the red as the internal energy rises. This suggests that species with a higher dissociation threshold, and with this a higher internal energy required, should show a more red-shifted IRMPD spectrum than species with a lower threshold. An illustrative example of this effect is found in the IRMPD spectrum of the para-amino benzoyl cation, $NH_2C_6H_4CO^+$ [131], a UV photolysis product of para-amino benzoic acid. Under influence of infrared multiple photon excitation, this species is found to dissociate into two competing channels, either losing only a CO unit or both, a CO and an HCN unit. The computed minimum energies required for dissociation into the two channels amounts to 3.5 and 4.9 eV, respectively. The loss of only HCN is not observed.

It is of course likely that the loss of CO and HCN is a sequential process i.e., that first CO is lost and then HCN. In many experiments where a cascade A → B → C is observed, it is difficult to draw conclusions, as absorption of additional photons by the intermediate (species B) can often not be excluded. Here, however, the C=O stretch mode is excited near $2150\,\mathrm{cm^{-1}}$, a region of the spectrum where no other fundamental mode absorbs. As the C=O unit will be the first to leave the ion, the intermediate ion can no longer absorb more photons at this wavelength.

The ions dissociating into the higher energy channel have a higher internal energy than those dissociating into the lower energy channel and hence, this should be reflected in the spectra recorded in the two channels. Fig. 9 shows the spectra of the CO stretching mode of $NH_2C_6H_4CO^+$ dissociating into the two channels which follow exactly the expected behavior. The CO stretching band was recorded with three different laser pulse energies as shown in the three different panels of Fig. 9 [131]. Three important observations can be made:

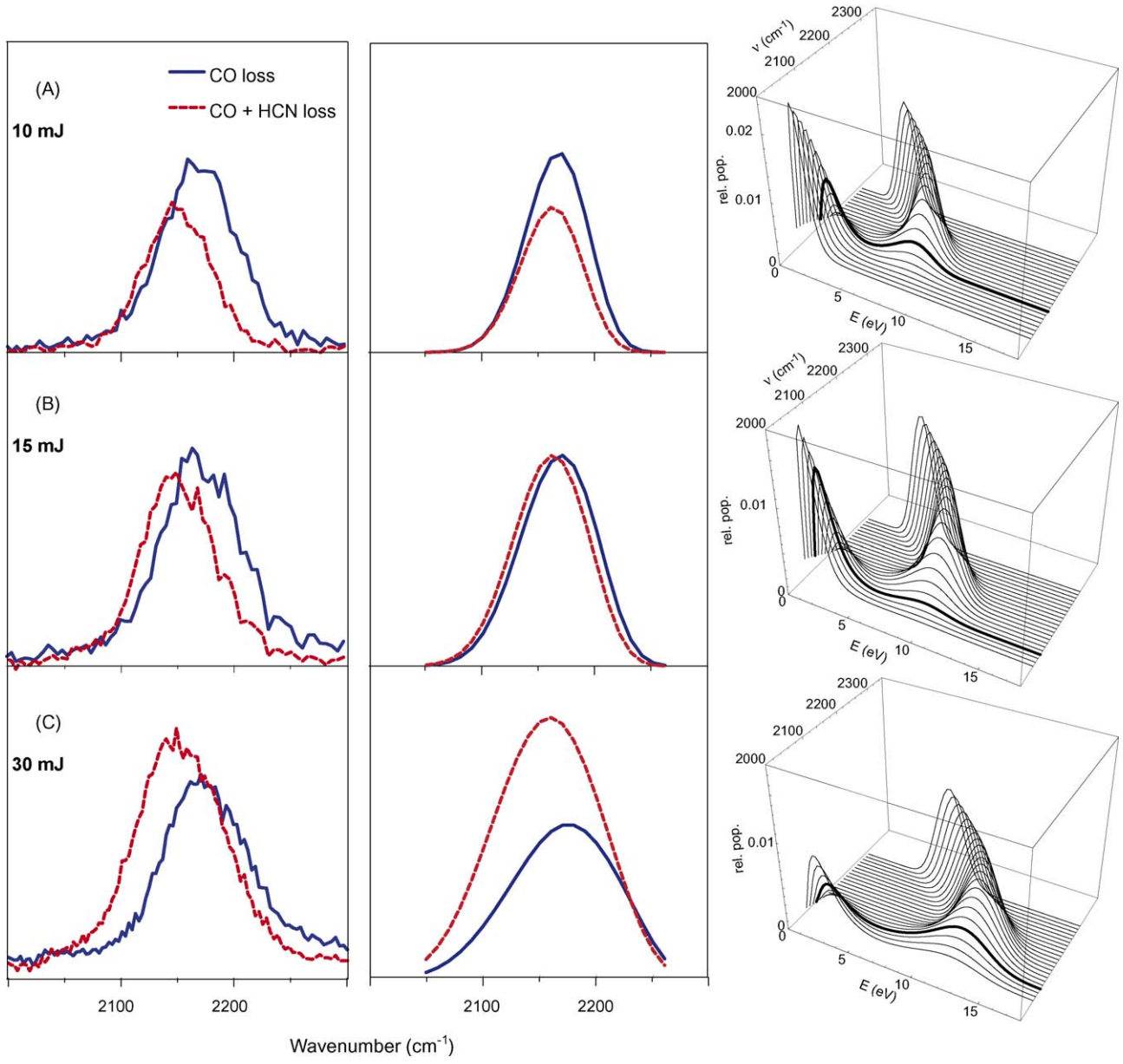


Fig. 9. IRMPD spectra of the para-amino benzoyl cation observed in two competing dissociation channels, loss of CO (solid) and loss of CO + HCN (dashed), where the latter channel obviously has a higher activation energy than the former. Anharmonic shifting causes a red shift that is higher for the higher energy channel. When the laser pulse energy is varied, the relative intensities observed in the two channels change, due to the cross-over in fragmentation rates as is well-known from unimolecular dissociation dynamics. The results of the model calculations are shown in the second column. The third column shows the internal energy distributions for different laser wavelengths around the CO stretching mode, given also for three different pulse energies (for interpretation of the references to color in this figure legend, the reader is referred to the web version of the article).

(1) the band center for the higher energy channel is redshifted with respect to that for the lower energy channel,
(2) as the pulse energy increases, the amount of fragmentation into the high energy channel increases as compared to that in the low energy channel, and
(3) the band positions of each individual channel do not shift noticably when changing the laser fluence.

This latter observations means that the average internal energy of the ions dissociating into either of the two channels does not change appreciable. What does change is the internal energy *distribution*, peaking at a higher value for higher pulse energies, so that a larger fraction of the ions fragment into the high energy channel. At the highest laser pulse energy it is seen that more ions fragment into the high energy channel than into the low energy one. This is due to the cross-over of dissociation rates as predicted by unimolecular dissociation theory.

To qualitatively model these observations using the mathematical methods described above, we use the DFT computed harmonic frequencies and integral absorption cross-sections, which amount to 1403 km/mol for the fundamental CO stretching mode. The DFT value for the vibrational frequency is adjusted to 2240 $cm^{-1}$ in order to fit the experimental spectra. The anharmonicity parameters of the CO-stretching mode are

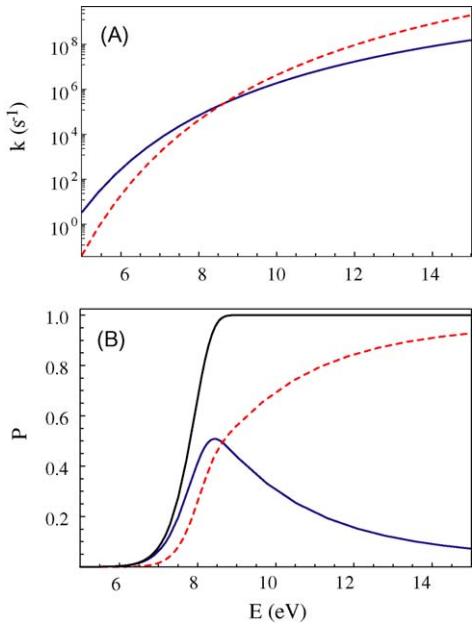


Fig. 10. Dissociation rate (A) and dissociation yield (B) of the PABz cation into the CO loss (blue) and CO + HCN loss (red) channels as a function of internal energy. The black curve in panel B represents the total dissociation yield (for interpretation of the references to color in this figure legend, the reader is referred to the web version of the article).

taken to best fit the experimental spectra: $a = 7.5\,\mathrm{cm}^{-1}$ and $b = 1.5\,\mathrm{cm}^{-1}$. As will be shown, these parameters give a reasonable agreement between simulations and experimental spectra.

The rates of dissociation into the two channels can be approximated by Arrhenius-like dependencies on the vibrational energy $E$: $k_i(E) = A_i \exp(-B_i/E)$. The constants $A_i$ were chosen to fit qualitatively the experimental spectra as $A_1 = 10^{12}\,\mathrm{s}$ for the low energy channel and $A_2 = 4.13 \times 10^{14}\,\mathrm{s}$ for the high energy channel. The constants $B_i$ were calculated from the energy thresholds to be $B_1 = 132\,\mathrm{eV}$ and $B_2 = 184\,\mathrm{eV}$ using the relationship between the dissociation energy $E_\mathrm{d}$ and parameter $B = (s_\mathrm{eff} - 1)E_\mathrm{d}$, where $s_\mathrm{eff}$ is the effective number of vibrational degrees of freedom taken for this case to be $s_\mathrm{eff} = 38.6$. The energy dependencies are plotted in Fig. 10, which shows that the dissociation rate into the first channel becomes lower than that into the second channel for excitation energies higher than 8.6 eV.

The dissociation yield is simulated assuming that the number of fragments is counted during a $\tau = 10$ μs time window after the laser pulse. Thus, the yield can be estimated as

$$w_i(E) = \frac{k_i(E)}{k_1(E) + k_2(E)}\{1 - \exp[-(k_1(E) + k_2(E))\tau]\} \quad (18)$$

The dependencies are plotted in Fig. 10. In the energy interval 3.5 eV< $E$ <8.6 eV, dissociation into the first channel dominates and for $E > 8.6$ eV, dissociation into the second channel dominates.

The evolution of population distribution was simulated by numerically solving the ordinary differential equations (see Eq. (11)). The initial population distribution before laser excitation was taken to be thermal at $T = 600\,\mathrm{K}$. The population distributions after excitation by the laser pulse with macropulse energies of 10, 15 and 30 mJ (approximately corresponding to fluences of 3, 4.5 and 9 J/cm$^2$, respectively) are shown in Fig. 9 (third column). The spectral dependencies of the dissociation yields were calculated taking into account that the laser beam has a Gaussian profile. Calculating now the dissociation yield averaging over the laser fluence spatial profile, gives the spectrum as shown in Fig. 9 (second column).

An interesting conclusion from these observations is that it is possible to "steer" the unimolecular dissociation reaction toward a specific reaction product by the appropriate choice of the infrared wavelength. Obviously, this approach is quite different from those applied in coherent control experiments [132–137], but the result is similar. The incoherent method applied here relies on the very specific internal energy distribution that is obtained, which determines the way the reaction proceeds. The shape of the distribution sensitively depends on the laser wavelength, bandwidth and pulse energy, as well as on the anharmonic properties of the molecule. Studies on more weakly bound systems, where various low energy dissociation channels are available, have shown that these effects occur regularly [138–140].

## 5. IR spectra of other mass-selected ionic species

In addition to the cationic PAH species described in chapter 3, several other interesting cationic species were investigated. An overview is given in this chapter.

### 5.1. Functionalized aromatics and their fragment ions

Fragmentation and rearrangement are commonly occurring phenomena when molecules or ions are being ionized or energized. While the molecular masses of those fragments can easily be determined, their structures are in general unknown. To characterize these fragment structures, one would like to record their infrared spectra.

In our present experimental setup, the low mass cutoff of the ion trap is used to mass-selectively isolate ions. Hence, it is only possible to isolate the heaviest species in the trap. Such experiments are facilitated when a species undergoes complete fragmentation after ionization. Shown in Fig. 2. is a mass spectrum, taken after irradiation of benzoic acid with UV ionization at 193 nm. Benzoic acid is found to completely fragment to cationic benzoyl, $C_6H_5CO$, and lower mass fragments [68]. This behavior can be rationalized by comparing the respective ionization and appearance energies (in eV) to the energy of a UV photon of 6.4 eV

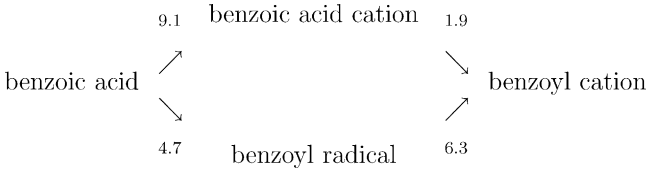


Formation of the benzoic acid cation would require a two-photon absorption process, whereas formation of the benzoyl

cation, via the benzoyl radical, can occur through two one-photon processes. Hence, only the lower route is observed, which allows the benzoyl cation at $m/z = 105$ to be isolated, and its spectrum subsequently to be recorded.

The neutral benzoyl radical is an interesting species with a long history. It was hypothesized already in 1789 by Lavoisier and it was discovered in 1832 by Wöhler and Justus von Liebig as one of the constituents of the oil of bitter almonds (benzaldehyde). Nonetheless, until recently, no experimental infrared spectra had been reported for the neutral radical nor for the closed-shell cationic species, which again indicates how (infrared) spectroscopy of polyatomic molecules has largely focused on stable neutral species.

Being a radical in the neutral state, the benzoyl cation has a closed-shell electronic structure and it can be considered as belonging to the class of reaction intermediates commonly referred to as carbocations [141]. In fact, two resonant structures are conceivable as shown in the inset of Fig. 11, a true carbocation type structure with the charge localized on the carbon atom and an oxonium ion structure, with a triple C≡O bond and the charge localized on the oxygen atom. Although the latter is known to be the more stable structure, not much spectroscopic evidence has been reported for gas-phase carbocations. The frequency of the CO stretching mode should be a sensitive probe to distinguish the two structures.

The IRMPD spectrum of the benzoyl cation, shown in the upper panel of Fig. 11, indeed agrees very well with the theoretically calculated spectrum for the oxonium ion type structure, i.e., a linear acylium type $-C{\equiv}O^+$ structure. The very intense CO stretching mode, recorded with FELIX lasing on the third harmonic mode, is found near 2200 $cm^{-1}$. The exact position of this band is determined by the resonance not only of the CO moiety, but of the entire conjugated π-system. This is evidenced by comparison of the spectrum to that of para-amino benzoyl [131], shown in the lower panel of Fig. 11. The addition of an amino group at the para position on the ring shifts the acylium C≡O stretch by about 50 $cm^{-1}$ to the red.

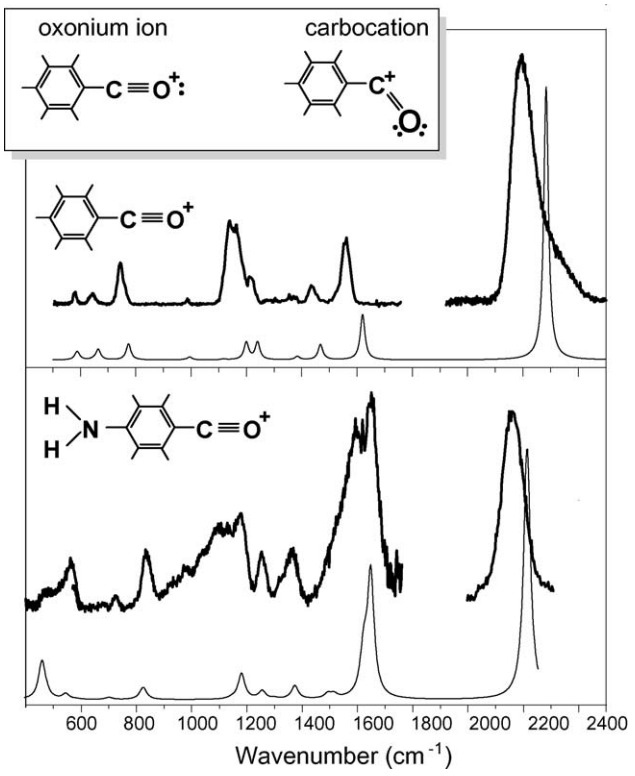


Fig. 11. IRMPD spectrum of cationic benzoyl (upper panel) and para-amino benzoyl (lower panel) compared with their calculated spectra. The ions are found to possess an oxonium ion type structure and the position of the acylium CO stretching band is sensitively determined by the degree of conjugation in the system.

### 5.2. Protonated molecules

Although protonation is obviously a process of key biochemical interest, until recently only very few gas-phase infrared spectroscopic studies of protonated systems had been reported. In fact, only relatively small prototypical protonated species had been investigated. In many cases, infrared spectroscopy allows for an unambiguous determination of the protonation site. In the 3 μm spectral range, the hydrogen stretching modes can be used as very diagnostic probes of the binding site, as has for instance been shown in the pioneering work of Dopfer and coworkers [24–26]. Though less intuitive, in the mid-infrared range, protonation also leads to very distinct spectroscopic probes. This is for instance shown by the work of Maître, Dopfer, Fornarini and various coworkers on benzene and some of its derivatives [142–144] as well as on different amino acids and dipeptides [50], using the CLIO free electron laser at Orsay, France [50].

In our experiments, we produce protonated species similar to the chemical ionization method described in Section 2.1.3. Depending on the gas-phase basicity of the low-mass ionic fragments and the proton affinity of the neutral target molecule, proton transfer can occur. Indeed, in Fig. 2 one observes not only the appearance of the benzoic acid cation ($m = 122$) but also of protonated benzoic acid ($m = 123$). The proton transfer rate is of the same order as the charge transfer rate [67], so that the cationic and protonated species are produced in similar amounts (see Fig. 2). The mass resolving power of the ion trap is insufficient to isolate protonated benzoic acid from its cationic brother. However, the two species show different dissociation channels (see Fig. 2) and thus, their infrared photodissociation spectra can be recorded simultaneously in a multiplexing fashion.

The mid-infrared spectrum of protonated benzoic acid is quite different from that of cationic benzoic acid, most importantly showing a red shift of the C≡O stretching mode of ≈ 200 $cm^{-1}$ [67]. This is rationalized by the attachment of the proton to the carbonyl oxygen atom, reducing the electron density in the CO bond substantially. Computationally, protonation at the carbonyl oxygen atom is indeed found to give the lowest energy structure. This method was also applied to indazole, belonging to the class of aromatic heterocyclic molecules. Here, the protonation site could also be unambiguously determined as the most electronegative site of the neutral molecule, the pyridinic nitrogen atom, and this structure also yields the lowest energy in a DFT calculation [145].

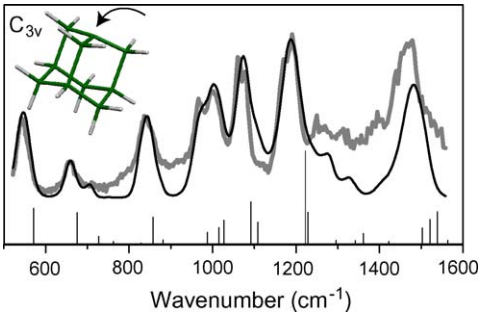


Fig. 12. IRMPD spectrum of cationic 1-adamantyl, $C_{10}H_{15}^{+}$ (grey). The DFT computed harmonic frequencies (stick spectrum) were used as input for a calculation of the MPD spectrum (black), where the anharmonicity parameters were used to fit the experiment. The $C_{3v}$ structure of the 1-adamantyl cation, where an H atom is detached from the position indicated with the arrow, is shown.

### 5.3. Non-aromatic species: adamantane

Non-aromatic organic species have the disadvantage that they cannot be UV photoionized so easily. Indeed, adamantane ($C_{10}H_{16}$), the smallest member of the molecular diamonds family, does not undergo ionization when exposed to the focused output of the ArF excimer laser. Therefore, ionization is again facillitated by charge transfer. Both adamantane and benzoic acid vapor is released into the vacuum chamber, in an approximately one-to-one mixing ratio. The excimer laser photolyses benzoic acid to form the low-mass charged fragments, as shown in Fig. 2. Since the IP of adamantane is comparable to that of benzoic acid, both molecules are ionized at a similar rate by charge transfer from the low-mass fragments [69]. Furthermore, as adamantane has a higher molecular weight than benzoic acid, the adamantane cation can easily be isolated in the trap by briefly raising the low mass cutoff.

Dehydrogenation of the adamantane cation is known to require only 1.4 eV [146], forming the closed-shell adamantyl cation ($C_{10}H_{15}^{+}$). Although the mass-resolving power of the ion trap is barely sufficient to determine whether the adamantane or adamantyl cation is present in the trap, the infrared spectrum shows good agreement with computations for the adamantyl cation. In fact, two isomeric forms of adamantyl exist and the infrared spectrum can be assigned to the $C_{3v}$ 1-adamantyl isomer [69], being lower in energy with respect to the $C_s$ 2-adamantyl isomer by 0.49 eV [146]. Applying the model described in Section 3, $a_i$ and $b_i$ parameters are determined for each vibrational band by fitting the modeled spectrum to the experimental one [69]. This procedure yields a convincing match (see Fig. 12), although at present there are no (experimental or computational) data available to verify the validity of the obtained values for the anharmonicity.

## 6. Conclusions and outlook

The coupling of an ion trap time-of-flight mass spectrometer to an infrared free electron laser allows the recording of IRMPD spectra of a variety of molecular ions over a wide spectral range. Hitherto, this method had only been applied over a small (and discontinuous) spectral range with the use of $CO_2$ lasers. The high pulse energies of the FEL are capable of dissociating strongly bound species, such as polyaromatics, via the absorption of tens to hundreds of IR photons in a single FEL macropulse. In contrast to direct absorption techniques (see e.g., [147,148]) or action spectroscopy techniques based on single photon absorption (such as the messenger technique [9] and laser induced reaction spectroscopy [149]), the resulting spectra may show manifestations of the multiple photon nature of the IRMPD technique. To investigate critically the extent of such effects on the IRMPD spectra, the excitation and fragmentation processes involved have been theoretically modeled. When required input parameters such as for example vibrational anharmonicities are known, calculated spectra match the experiment quite well. On the other hand, however, we have empirically found that in most cases, the IRMPD spectra appear to be very close to the corresponding (calculated) linear absorption spectra.

These considerations make IRMPD spectroscopy of trapped ionic species a valuable tool in the structural characterization of ionic species. As compared to other techniques, mainly the rare gas tagging messenger technique (that has in fact been applied to some small PAH cations in our lab [96,97]), the IRMPD method does not require a molecular beam expansion nor complex two-color REMPI schemes for preparation of the ions. Tagging with small molecular species that bind more strongly, has the disadvantage of overlapping vibrational bands in the infrared spectral range targeted here. As compared to molecular beam techniques, methods based on ion trapping instruments offer various possibilities for ion manipulation, such as production and isolation of specific parent ion species. In general, one could say that the IRMPD method has been very successful for large molecular systems and clusters, whereas direct absorption and messenger spectroscopy techniques have mainly been applied to relatively small systems.

Hence, combined with more advanced mass-spectrometric techniques, the methods described in this work hold great promise for the structural characterization of a wealth of charged gas-phase species. When we started our spectroscopic investigations of gas-phase ions, FELIX was the only FEL used to this end. By now, similar experiments are performed at CLIO in Orsay, France, and several other FEL facilities are in the design and planning phase. We believe that the future is bright for experiments on gas-phase ions using IR-FELs.

## Acknowledgments

Over the course of the past 7 years, several students and postdocs in our laboratory have contributed to the work described in this paper. We would like to particularly thank David T. Moore and Nick Polfer. The success of this project would not have been possible without the expert assistance from the FELIX staff, particularly Lex van der Meer, Britta Redlich, Rene van Buuren, Wim Mastop, and Peter Delmee. The technical assistance from André van Roij and Jan Pluijgers in the construction of the ion trap setup is gratefully acknowledged. This work is part of the research program of FOM, which is financially supported by the Nederlandse Organisatie voor Wetenschappelijk Onderzoek (NWO).

## References


[1] R.D. van Zee, J.P. Looney (Eds.), Cavity-enhanced Spectroscopies, Experimental methods in Physical Sciences, vol. 40, Academic Press, San Diego, USA, 2002.
[2] H.A. Schwarz, J. Chem. Phys. 67 (1977) 5525.
[3] T. Oka, Phys. Rev. Lett. 45 (1980) 531.
[4] J.P. Bekooy, P. Verhoeve, W.L. Meerts, A. Dymanus, J. Chem. Phys. 82 (1985) 3868.
[5] P. Verhoeve, M. Versluis, J.J. ter Meulen, A. Dymanus, Chem. Phys. Lett. 161 (1989) 195.
[6] C.S. Gudeman, M.H. Begemann, J. Pfaff, R.J. Saykally, Phys. Rev. Lett. 50 (1983) 727.
[7] E.R. Keim, M.L. Polak, J.C. Owrutsky, J.V. Coe, R.J. Saykally, J. Chem. Phys. 93 (1990) 3111.
[8] M.A. Duncan, Int. J. Mass Spectrom. 200 (2000) 545.
[9] M. Okumura, L.I. Yeh, Y.T. Lee, J. Chem. Phys. 83 (1985) 3705.
[10] M. Okumura, L.I. Yeh, J.D. Myers, Y.T. Lee, J. Chem. Phys. 85 (1986) 2328.
[11] L.I. Yeh, M. Okumura, J.D. Myers, J.M. Price, Y.T. Lee, J. Chem. Phys. 91 (1989) 7319.
[12] V.N. Bagratashvili, V.S. Letokhov, A.A. Makarov, E.A. Ryabov, Multiple Photon Infrared Laser Photophysics and Photochemistry, Gordon and Breach, New York, 1985.
[13] M. Kamioka, S. Arai, Y. Ishikawa, S. Isomura, N. Takamiya, Chem. Phys. Lett. 119 (1985) 357.
[14] A.K. Petrov, E.N. Chesnokov, S.R. Gorelik, K.D. Straub, E.B. Szarmes, J.M.J. Madey, J. Phys. Chem. A 101 (1997) 7200.
[15] S. Kuribayashi, T. Tomimasu, S. Kawanishi, S. Arai, Appl. Phys. B 65 (1997) 393.
[16] G.N. Makarov, A.N. Petin, Chem. Phys. 266 (2001) 125.
[17] J. Makowe, O.V. Boyarkin, T.R. Rizzo, J. Phys. Chem. A 106 (2002) 5221.
[18] J.I. Steinfeld, An Introduction to Modern Molecular Spectroscopy, 2nd ed., MIT Press, Cambridge, MA, 1986 pp. 426-429.
[19] S.K. Shin, J.L. Beauchamp, J. Am. Chem. Soc. 112 (1990) 2057.
[20] S.K. Shin, J.L. Beauchamp, J. Am. Chem. Soc. 112 (1990) 2066.
[21] D.M. Peiris, M.A. Cheeseman, R. Ramanathan, J.R. Eyler, J. Phys. Chem. 97 (1993) 7839.
[22] J.L. Stephenson, M.M. Booth, J.A. Shalosky, J.R. Eyler, R.A. Yost, J. Am. Soc. Mass Spectrom. 5 (1994) 886.
[23] D.A. Kirkwood, A.J. Stace, J. Am. Chem. Soc. 120 (1999) 12316.
[24] N. Solcà, O. Dopfer, Chem. Phys. Lett. 342 (2001) 191.
[25] N. Solcà, O. Dopfer, Angew. Chem. Int. Ed. Engl. 41 (2002) 3628.
[26] N. Solcà, O. Dopfer, J. Am. Chem. Soc. 125 (2003) 1421.
[27] E.J. Bieske, O. Dopfer, Chem. Rev. 100 (2000) 3963.
[28] D.A. Wild, Z.M. Loh, E.J. Bieske, Int. J. Mass Spectrom. 220 (2002) 273.
[29] E.J. Bieske, Chem. Soc. Rev. 32 (2003) 231.
[30] H. Kawamata, T. Maeyama, N. Mikami, Chem. Phys. Lett. 370 (2003) 535.
[31] M. Miyazaki, A. Fujii, T. Ebata, N. Mikami, J. Phys. Chem. A 108 (2004) 10656.
[32] S. Enomoto, M. Miyazaki, A. Fujii, N. Mikami, J. Phys. Chem. A 109 (2005) 9471.
[33] M. Miyazaki, A. Fujii, T. Ebata, N. Mikami, Science 304 (2004) 1134.
[34] A. Fujii, S. Enomoto, M. Miyazaki, N. Mikami, J. Phys. Chem. A 109 (2005) 138.
[35] J.M. Headrick, E.G. Diken, R.S. Walters, N.I. Hammer, R.A. Christie, J. Cui, E.M. Myshakin, M.A. Duncan, M.A. Johnson, K.D. Jordan, Science 308 (2005) 1765.
[36] E.G. Diken, J.M. Headrick, J.R. Roscioli, J.C. Bopp, M.A. Johnson, A.B. McCoy, J. Phys. Chem. A 109 (2005) 1487.
[37] R.S. Walters, E. Dinesh Pillai, M.A. Duncan, J. Am. Chem. Soc. 127 (2005) 16599.
[38] N.R. Walker, R.S. Walters, M.A. Duncan, New J. Chem. 29 (2005) 1495.
[39] O.M. Cabarcos, C.J. Weinheimer, J.M. Lisy, J. Chem. Phys. 110 (1999) 8429.
[40] T.D. Vaden, J.M. Lisy, J. Chem. Phys. 120 (2004) 721.
[41] A. Kamariotis, O.V. Boyarkin, S.R. Mercier, R.D. Beck, M.F. Bush, E.R. Williams, T.R. Rizzo, J. Am. Chem. Soc. 128 (2006) 905.
[42] H.B. Oh, H.Y. Hwang, H.L. Zhai, K. Breuker, V. Zabrouskov, B.K. Carpenter, F.W. McLafferty, J. Am. Chem. Soc. 127 (2005) 4076.
[43] B.E. Newnam, J.W. Early, J.L. Lyman, Nucl. Instr. Meth. Phys. Res. A 341 (1994) 142.
[44] J.L. Lyman, B.E. Newnam, J.W. Early, A.F.G. van der Meer, J. Phys. Chem. A 101 (1997) 49.
[45] J. Oomens, A.J.A. van Roij, G. Meijer, G. von Helden, Astrophys. J. 542 (2000) 404.
[46] D.T. Moore, J. Oomens, L. van der Meer, G. von Helden, G. Meijer, J. Valle, A.G. Marshall, J.R. Eyler, ChemPhysChem. 5 (2004) 740.
[47] T.D. Fridgen, L. MacAleese, P. Maître, T.B. McMahon, P. Boissel, J. Lemaire, Phys. Chem. Chem. Phys. 7 (2005) 2747.
[48] K.R. Asmis, N.L. Pivonka, G. Santambrogio, M. Brummer, C. Kaposta, D.M. Neumark, L. Wöste, Science 299 (2003) 1375.
[49] T.D. Fridgen, T.B. McMahon, L. MacAleese, J. Lemaire, P. Maitre, J. Phys. Chem. A 108 (2004) 9008.
[50] B. Lucas, G. Grégoire, P. Maître, F. Glotin, J.P. Schermann, C. Desfrancois, Int. J. Mass Spectrom. 243 (2005) 105.
[51] B. Lucas, G. Grégoire, P. Maître, J.M. Ortega, A. Rupenyan, B. Reimann, J.P. Schermann, C. Desfrancois, Phys. Chem. Chem. Phys. 6 (2004) 2659.
[52] N.C. Polfer, B. Paizs, L.C. Snoek, I. Compagnon, S. Suhai, G. Meijer, G. von Helden, J. Oomens, J. Am. Chem. Soc. 127 (2005) 8571.
[53] A. Simon, W. Jones, J.M. Ortega, P. Boissel, J. Lemaire, P. Maître, J. Am. Chem. Soc. 126 (2004) 11666.
[54] J. Oomens, D.T. Moore, G. von Helden, G. Meijer, R.C. Dunbar, J. Am. Chem. Soc. 126 (2004) 724.
[55] D.T. Moore, J. Oomens, J.R. Eyler, G. von Helden, G. Meijer, R.C. Dunbar, J. Am. Chem. Soc. 127 (2005) 7243.
[56] J. Oomens, N. Polfer, D.T. Moore, L. van der Meer, A.G. Marshall, J.R. Eyler, G. Meijer, G. von Helden, Phys. Chem. Chem. Phys. 7 (2005) 1345.
[57] N.L. Pivonka, C. Kaposta, G. von Helden, G. Meijer, L. Wöste, D.M. Neumark, K.R. Asmis, J. Chem. Phys. 117 (2002) 6493.
[58] D.T. Moore, J. Oomens, J.R. Eyler, G. Meijer, G. von Helden, D.P. Ridge, J. Am. Chem. Soc. 126 (2004) 14726.
[59] K.R. Asmis, G. Santambrogio, M. Brümmer, J. Sauer, Angew. Chem. Int. Ed. 44 (2005) 2.
[60] W.B. Colson, E.D. Johnson, M.J. Kelley, H.A. Schwettman, Phys. Today 55 (2002) 35.
[61] G.S. Edwards, S.J. Allen, R.F. Haglund, R.J. Nemanich, B. Redlich, J.D. Simon, W.-C. Yang, Photochem. Photobiol. 81 (2005) 711.
[62] P. Luchini, H. Motz, Undulators and Free Electron Lasers, Oxford university Press, Oxford, UK, 1990.
[63] H.P. Freund, T.M. Antonsen Jr., Principles of Free Electron Lasers, Chapman and Hall, London, UK, 1992.
[64] D. Oepts, A.F.G. van der Meer, P.W. van Amersfoort, Infrared Phys. Technol. 36 (1995) 297.
[65] S.M. Michael, M. Chien, D.M. Lubman, Rev. Sci. Instrum. 63 (1992) 4277.
[66] W. Paul, Rev. Mod. Phys. 62 (1990) 531.
[67] J. Oomens, G. von Helden, G. Meijer, J. Phys. Chem. A 108 (2004) 8273.
[68] J. Oomens, J.M. Bakker, B.G. Sartakov, G. Meijer, G. von Helden, Chem. Phys. Lett. 367 (2003) 576.
[69] N. Polfer, B.G. Sartakov, J. Oomens, Chem. Phys. Lett. 400 (2004) 201.
[70] A.D. Becke, J. Chem. Phys. 98 (1993) 5648.
[71] C. Lee, W. Yang, R. Parr, Phys. Rev. B 37 (1988) 785.
[72] M.J. Frisch, G.W. Trucks, H.B. Schlegel, G.E. Scuseria, M.A. Robb, J.R. Cheeseman, V.G. Zakrzewski, J.A. Montgomery, Jr., R.E. Stratmann, J.C. Burant, S. Dapprich, J.M. Millam, A.D. Daniels, K.N. Kudin, M.C. Strain, O. Farkas, J. Tomasi, V. Barone, M. Cossi, R. Cammi, B. Mennucci, C. Pomelli, C. Adamo, S. Clifford, J. Ochterski, G.A. Petersson, P.Y. Ayala, Q. Cui, K. Morokuma, D.K. Malick, A.D. Rabuck, K. Raghavachari, J.B. Foresman, J. Cioslowski, J.V. Ortiz, A.G. Baboul, B.B. Stefanov, G. Liu, A. Liashenko, P. Piskorz, I. Komaromi, R. Gomperts, R.L. Martin, D.J. Fox, T. Keith, M.A. Al-Laham, C.Y. Peng, A. Nanayakkara, C. Gonzalez, M. Challacombe, P.M.W. Gill, B. Johnson, W. Chen, M.W. Wong, J.L. Andres, C. Gonzalez, M. Head-Gordon, E.S. Replogle, J.A. Pople, Gaussian 98, Rev. A.7, Gaussian, Inc., Pittsburgh, PA, 1998.
[73] S.R. Langhoff, J. Phys. Chem. 100 (1996) 2819.

[74] C.W. Bauschlicher, S.R. Langhoff, Spectrochim. Acta A 53 (1997) 1225.
[75] C.W. Bauschlicher Jr., D.M. Hudgins, L.J. Allamandola, Theor. Chem. Acc. 103 (1999) 154.
[76] J. Oomens, G. Meijer, G. von Helden, J. Phys. Chem. A 105 (2001) 8302.
[77] J. Oomens, B.G. Sartakov, A.G.G.M. Tielens, G. Meijer, G. von Helden, Astrophys. J. 560 (2001) 99.
[78] J. Banisaukas, J. Szczepanski, J. Eyler, M. Vala, S. Hirata, M. Head-Gordon, J. Oomens, G. Meijer, G. von Helden, J. Phys. Chem. A 107 (2003) 782.
[79] A. Leger, J.L. Puget, Astron. Astrophys. 137 (1984) 5.
[80] L.J. Allamandola, A.G.G.M. Tielens, J.R. Barker, Astrophys. J. Lett. 290 (1985) 25.
[81] L.J. Allamandola, A.G.G.M. Tielens, J.R. Barker, Astrophys. J. Suppl. Ser. 71 (1989) 733.
[82] D.J. Cook, S. Schlemmer, N. Balucani, D.R. Wagner, B. Steiner, R.J. Saykally, Nature 380 (1996) 227.
[83] H.-S. Kim, D.R. Wagner, R.J. Saykally, Phys. Rev. Lett. 86 (2001) 5691.
[84] A.G.G.M. Tielens, The Physics and Chemistry of the Interstellar Medium, Cambridge University Press, Cambridge, UK, 2005.
[85] W.A. Schutte, A.G.G.M. Tielens, L.J. Allamandola, Astrophys. J. 415 (1993) 397.
[86] D.J. Cook, R.J. Saykally, Astrophys. J. 493 (1998) 793.
[87] E.L.O. Bakes, A.G.G.M. Tielens, C.W. Bauschlicher Jr., Astrophys. J. 556 (2001) 501.
[88] C. Joblin, A.G.G.M. Tielens, T.R. Geballe, D.H. Wooden, Astrophys. J. Lett. 460 (1996) 119.
[89] G.C. Sloan, T.L. Hayward, L.J. Allamandola, J.D. Bregman, B. DeVito, D.M. Hudgins, Astrophys. J. Lett. 513 (1999) 65.
[90] J. Szczepanski, D. Roser, W. Personnette, M. Eyring, R. Pellow, M. Vala, J. Phys. Chem. 96 (1992) 7876.
[91] J. Szczepanski, M. Vala, Astrophys. J. 414 (1993) 646.
[92] D.M. Hudgins, S.A. Sandford, L.J. Allamandola, J. Phys. Chem. 98 (1994) 4243.
[93] D.M. Hudgins, L.J. Allamandola, J. Phys. Chem. 99 (1995) 3033.
[94] D.M. Hudgins, C.W. Bauschlicher Jr., L.J. Allamandola, J.C. Fetzer, J. Phys. Chem. A 104 (2000) 3655.
[95] C. Joblin, L. d'Hendecourt, A. Léger, D. Défourneau, Astron. Astrophys. 281 (1994) 923.
[96] H. Piest, G. von Helden, G. Meijer, Astrophys. J. Lett. 520 (1999) 75.
[97] J.A. Piest, J. Oomens, J. Bakker, G. von Helden, G. Meijer, Spectrochim. Acta A 57 (2001) 717.
[98] J. Oomens, A.G.G.M. Tielens, B.G. Sartakov, G. von Helden, G. Meijer, Astrophys. J. 591 (2003) 968.
[99] R.G. Satink, H. Piest, G. von Helden, G. Meijer, J. Chem. Phys. 111 (1999) 10750.
[100] O. Dopfer, R.V. Olkhov, J.P. Maier, J. Chem. Phys. 111 (1999) 10754.
[101] J.M. Bakker, R.G. Satink, G. von Helden, G. Meijer, Phys. Chem. Chem. Phys. 4 (2002) 24.
[102] D.M. Hudgins, L.J. Allamandola, Astrophys. J. Lett. 516 (1999) 41.
[103] D.J. De Frees, M.D. Miller, D. Talbi, F. Pauzat, Y. Ellinger, Astrophys. J. 408 (1993) 530.
[104] M.J. Dibben, D. Kage, J. Szczepanski, J.R. Eyler, M. Vala, J. Phys. Chem. A 105 (2001) 6024.
[105] J. Szczepanski, M.J. Dibben, W. Pearson, J.R. Eyler, M. Vala, J. Phys. Chem. A 105 (2001) 9388.
[106] J.J. Valle, J.R. Eyler, J. Oomens, D.T. Moore, A.F.G. van der Meer, G. von Helden, G. Meijer, C.L. Hendrickson, A.G. Marshall, G.T. Blakney, Rev. Sci. Instrum. 76 (2005) 023103.
[107] J. Banisaukas, J. Szczepanski, J. Eyler, M. Vala, J. Phys. Chem. A 108 (2004) 3723.
[108] H.A. Jahn, E. Teller, Proc. Roy. Soc. (London) A161 (1937) 220.
[109] G. Herzberg, Molecular Spectra and Molecular Structure—Electronic Spectra and Electronic Structure of Polyatomic Molecules, vol. III, Van Nostrand Reinhold Company Inc., 1966.
[110] R. Lindner, K. Müller-Dethlefs, E. Wedum, K. Haber, E.R. Grant, Science 271 (1996) 1698.
[111] B.E. Applegate, T.A. Barckholtz, T.A. Miller, Chem. Soc. Rev. 32 (2003) 38.
[112] B.E. Applegate, T.A. Miller, J. Chem. Phys. 117 (2002) 10654.
[113] T. Kato, K. Yoshizawa, T. Yamabe, J. Chem. Phys. 110 (1999) 249.
[114] T. Keszthelyi, G. Balakrishnan, R. Wilbrandt, W.A. Yee, F. Negri, J. Phys. Chem. A 104 (2000) 9121.
[115] T. Kato, T. Yamabe, Chem. Phys. Lett. 403 (2005) 113.
[116] J.G. Black, E. Yablonovitch, N. Bloembergen, S. Mukamel, Phys. Rev. Lett. 38 (1977) 1131.
[117] E.R. Grant, P.A. Schulz, Aa.S. Sudbo, Y.R. Shen, Y.T. Lee, Phys. Rev. Lett. 40 (1978) 115.
[118] K.K. Lehmann, G. Scoles, B.H. Pate, Annu. Rev. Phys. Chem. 45 (1994) 241.
[119] P.M. Felker, A.H. Zewail, J. Chem. Phys. 82 (1985) 2975.
[120] A. Callegari, U. Merker, P. Engels, H.K. Srivastava, K.K. Lehmann, G. Scoles, J. Chem. Phys. 113 (2000) 10583.
[121] M. Bixon, J. Jortner, J. Chem. Phys. 48 (1986) 715.
[122] V.M. Akulin, S.S. Alimpiev, N.V. Karlov, A.M. Prokhorov, B.G. Sartakov, E.M. Khokhlov, JETP Lett. 25 (1977) 400.
[123] P.C. Haarhoff, Mol. Phys. 7 (1963) 101.
[124] S.E. Stein, B.S. Rabinovitch, J. Chem. Phys. 58 (1973) 2438.
[125] See e.g., C. Cohen-Tannoudji, B. Diu, F. Laloë, Quantum Mechanics, vol. I, Chapter V, John Wiley & Sons, New York, 1977.
[126] S.S. Alimpiev, B.O. Zirkin, B.G. Sartakov, E.M. Khokhlov, Sov. Phys. JETP 56 (1982) 943.
[127] J. Oomens, G. von Helden, G. Meijer, Int. J. Mass Spectrom. 221 (2002) 163.
[128] Y. Hu, B. Hadas, M. Davidovitz, B. Balta, C. Lifshitz, J. Phys. Chem. A 107 (2003) 6507.
[129] C. Joblin, P. Boissel, A. Léger, L. d'Hendecourt, D. Défourneau, Astron. Astrophys. 299 (1995) 835.
[130] H.W. Jochims, E. Rühl, H. Baumgärtel, S. Tobita, S. Leach, Astrophys. J. 420 (1994) 307.
[131] J. Oomens, D.T. Moore, G. Meijer, G. von Helden, Phys. Chem. Chem. Phys. 6 (2004) 710.
[132] P. Brumer, M. Shapiro, Chem. Phys. Lett. 126 (1986) 541.
[133] D.J. Tannor, S.A. Rice, J. Chem. Phys. 83 (1985) 5013.
[134] K. Bergmann, H. Theuer, B.W. Shore, Rev. Mod. Phys. 70 (1998) 1003.
[135] K. Bergmann, G. Meijer, J. Reuss, Opt. Expr. 4 (1999) 44.
[136] H. Rabitz, R. de Vivie-Riedle, M. Motzkus, K. Kompa, Science 288 (2000) 824.
[137] M. Shapiro, P. Brumer, Rep. Prog. Phys. 66 (2003) 859.
[138] S.A. Nizkorodov, O. Dopfer, T. Ruchti, M. Meuwly, J.P. Maier, E.J. Bieske, J. Phys. Chem. 99 (1995) 17118.
[139] N.C. Polfer, J.J. Valle, D.T. Moore, J. Oomens, J.R. Eyler, B. Bendiak, Anal. Chem. 78 (2006) 670.
[140] R.C. Dunbar, D.T. Moore, J. Oomens, J. Phys. Chem. A, in press (doi:10.1021/jp0566921).
[141] G.A. Olah, B.G. Malmström (Eds.), Nobel Lectures, Chemistry, World Scientific Publishing Co., Singapore, 1997.
[142] W. Jones, P. Boissel, B. Chiavarino, M.E. Crestoni, S. Fornarini, J. Lemaire, P. Maitre, Angew. Chem. Int. Ed. Engl. 42 (2003) 2057.
[143] O. Dopfer, N. Solcà, J. Lemaire, P. Maitre, M.E. Crestoni, S. Fornarini, J. Phys. Chem. A 109 (2005) 7881.
[144] O. Dopfer, J. Lemaire, P. Maître, B. Chiavarino, M.E. Crestoni, S. Fornarini, Int. J. Mass Spectrom. 249/250 (2006) 149.
[145] J. Oomens, G. Meijer, G. von Helden, Int. J. Mass Spectrom. 249/250 (2006) 199.
[146] G. Yan, N.R. Brinkmann, H.F. Schaefer, J. Phys. Chem. A 107 (2003) 9479.
[147] D.T. Anderson, S. Davis, T.S. Zwier, D.J. Nesbitt, Chem. Phys. Lett. 258 (1996) 207.
[148] T. Speck, H. Linnartz, J.P. Maier, J. Chem. Phys. 107 (1997) 8706.
[149] O. Asvany, P. Kumar, B. Redlich, I. Hegemann, S. Schlemmer, D. Marx, Science 309 (2005) 1219.